Article

Cell Metabolism

Inhibition of Mevalonate Pathway Prevents Adipocyte Browning in Mice and Men by Affecting Protein Prenylation

Graphical Abstract

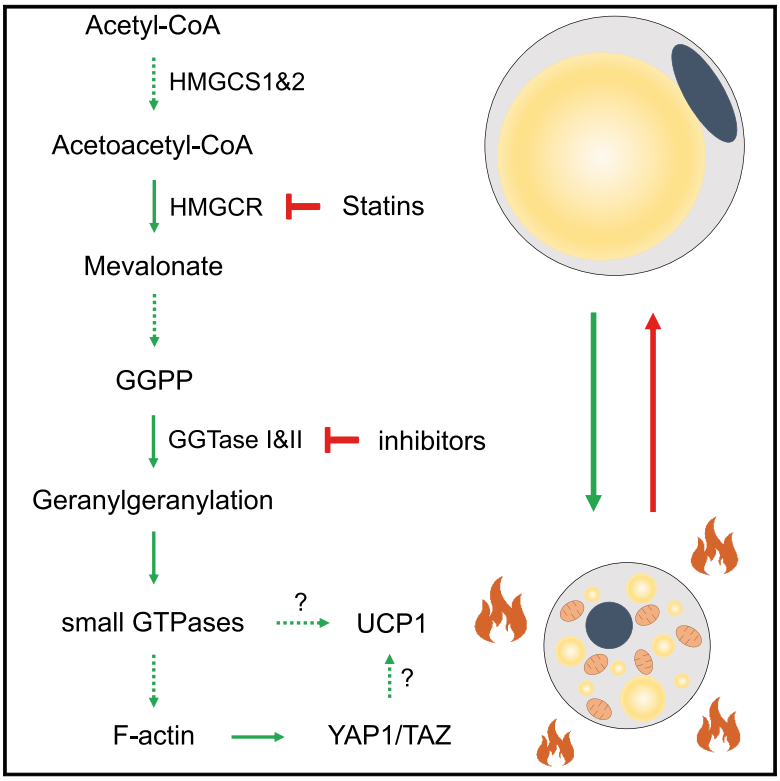

Authors

Miroslav Balaz, Anton S. Becker, Lucia Balazova, ..., Matthias Johannes Betz, Irene A. Burger, Christian Wolfrum

Correspondence

matthias.betz@usb.ch (M.J.B.), irene.burger@usz.ch (I.A.B.), christian-wolfrum@ethz.ch (C.W.)

In Brief

Through genetic and pharmacological *in vivo* and *in vitro* approaches, Balaz et al. show that the mevalonate pathway is important for adipocyte browning. The importance of this pathway is supported by a retrospective clinical study and a small volunteer trial with fluvastatin. The authors identify geranylgeranyl pyrophosphate as the key mevalonate intermediate driving adipocyte browning.

Highlights

- The mevalonate pathway is important for adipose tissue browning in mouse and human
- Statin use is inversely correlated with brown fat activity in humans
- Geranylgeranylation of small GTP-binding proteins promotes adipocyte browning
- Small GTP-binding proteins regulate F-actin formation and YAP1/TAZ stability

Balaz et al., 2019, Cell Metabolism *29*, 901–916
April 2, 2019
https://doi.org/10.1016/j.cmet.2018.11.017

CellPress

Cell Metabolism
Article

Inhibition of Mevalonate Pathway Prevents Adipocyte Browning in Mice and Men by Affecting Protein Prenylation

Miroslav Balaz,[1,14] Anton S. Becker,[1,2,3,14] Lucia Balazova,[1] Leon Straub,[1] Julian Müller,[3] Gani Gashi,[4] Claudia Irene Maushart,[4] Wenfei Sun,[1] Hua Dong,[1] Caroline Moser,[1] Carla Horvath,[1] Vissarion Efthymiou,[1] Yael Rachamin,[1] Salvatore Modica,[1] Caroline Zellweger,[3] Sara Bacanovic,[3] Patrik Stefanicka,[5] Lukas Varga,[5,6] Barbara Ukropcova,[6,7] Milan Profant,[5] Lennart Opitz,[8] Ez-Zoubir Amri,[9] Murali K. Akula,[10] Martin Bergo,[10,11] Jozef Ukropec,[6] Christian Falk,[12] Nicola Zamboni,[13] Matthias Johannes Betz,[4,*] Irene A. Burger,[3,*] and Christian Wolfrum[1,15,*]

[1]Institute of Food, Nutrition, and Health, ETH Zürich, Schorenstrasse 16, Schwerzenbach 8603, Switzerland
[2]Institute of Diagnostic and Interventional Radiology, University Hospital of Zürich, Zürich, Switzerland
[3]Department of Nuclear Medicine, University Hospital of Zürich, Rämistrasse 100, Zürich 8091, Switzerland
[4]Department of Endocrinology, Diabetology, and Metabolism, University Hospital of Basel, Petersgraben 4, Basel 4031, Switzerland
[5]Department of Otorhinolaryngology – Head and Neck Surgery, Faculty of Medicine and University Hospital, Comenius University, Bratislava, Slovakia
[6]Institute of Experimental Endocrinology, Biomedical Research Center at the Slovak Academy of Sciences, Bratislava, Slovakia
[7]Institute of Pathological Physiology, Faculty of Medicine, Comenius University, Bratislava, Slovakia
[8]Functional Genomics Center Zürich, ETH Zürich/University of Zürich, Zürich, Switzerland
[9]Université Côte d'Azur, CNRS, Inserm, iBV, Nice, France
[10]Sahlgrenska Cancer Center, Department of Medicine, University of Gothenburg, Gothenburg, Sweden
[11]Department of Biosciences and Nutrition, Karolinska Institute, Huddinge, Sweden
[12]Department of Medical Data Management, University Hospital of Zürich, Zürich, Switzerland
[13]Department of Biology, Institute of Molecular Systems Biology, ETH Zürich, Zürich, Switzerland
[14]These authors contributed equally
[15]Lead Contact
*Correspondence: matthias.betz@usb.ch (M.J.B.), irene.burger@usz.ch (I.A.B.), christian-wolfrum@ethz.ch (C.W.)
https://doi.org/10.1016/j.cmet.2018.11.017

SUMMARY

Recent research focusing on brown adipose tissue (BAT) function emphasizes its importance in systemic metabolic homeostasis. We show here that genetic and pharmacological inhibition of the mevalonate pathway leads to reduced human and mouse brown adipocyte function *in vitro* and impaired adipose tissue browning *in vivo*. A retrospective analysis of a large patient cohort suggests an inverse correlation between statin use and active BAT in humans, while we show in a prospective clinical trial that fluvastatin reduces thermogenic gene expression in human BAT. We identify geranylgeranyl pyrophosphate as the key mevalonate pathway intermediate driving adipocyte browning *in vitro* and *in vivo*, whose effects are mediated by geranylgeranyltransferases (GGTases), enzymes catalyzing geranylgeranylation of small GTP-binding proteins, thereby regulating YAP1/TAZ signaling through F-actin modulation. Conversely, adipocyte-specific ablation of GGTase I leads to impaired adipocyte browning, reduced energy expenditure, and glucose intolerance under obesogenic conditions, highlighting the importance of this pathway in modulating brown adipocyte functionality and systemic metabolism.

INTRODUCTION

Brown adipose tissue (BAT) is considered the main thermogenic organ in newborn mammals and hibernating rodents due to its capacity to dissipate chemical energy in the form of heat (Cannon and Nedergaard, 2004). Apart from the classical interscapular BAT (iBAT), brown adipocytes are also present within specific white adipose tissues (WATs) (Frontini et al., 2013). These cells, morphologically resembling brown adipocytes, are referred to as brite or beige adipocytes, and their formation can be induced by certain environmental, hormonal, and pharmacological stimuli (Frontini et al., 2013; Rosenwald et al., 2013; Shi and Collins, 2017). Under specific conditions, physiologically relevant amounts of BAT can be found also in adult humans (Cypess et al., 2009; Nedergaard et al., 2007; van Marken Lichtenbelt et al., 2009). BAT can be activated in healthy lean subjects and its activity can be measured by indirect calorimetry or by [^{18}F]fluorodeoxyglucose (FDG)-positron emission tomography (PET)/computed tomography (CT) (Cypess et al., 2015). BAT is dependent on glucose and free fatty acids (FFAs) as substrates for thermogenesis, suggesting a potential role for BAT in systemic glucose and lipid homeostasis (Bartelt et al., 2011; Chondronikola et al., 2014; Orava et al., 2011; Ouellet et al.,

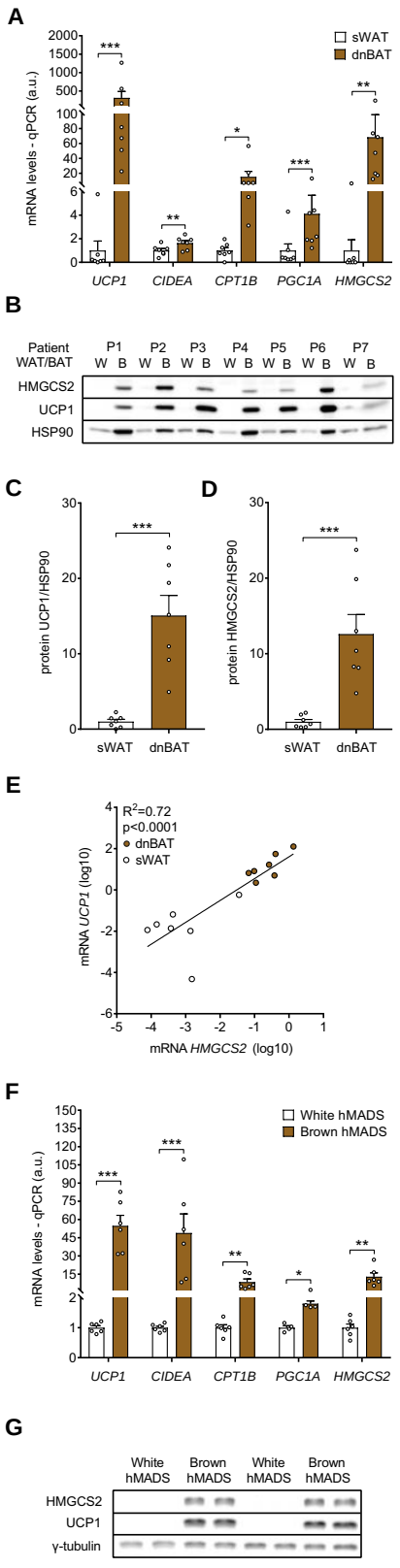

Figure 1. HMGCS2 Is Enriched in Human BAT

(A) Expression of brown adipocyte markers in human deep neck BAT (dnBAT) and subcutaneous WAT (sWAT) biopsies (n = 7).

(B–D) (B) Representative western blot (WB) and quantification of (C) UCP1 and (D) HMGCS2 in deep neck BAT and subcutaneous WAT (n = 7).

(E) Correlation between *UCP1* and *HMGCS2* mRNA in deep neck BAT and subcutaneous WAT (n = 7).

(F) Expression of brown adipocyte markers in hMADS cells (n = 4–6).

(G) Representative WB showing UCP1 and HMGCS2 levels in hMADS cells (n = 4).

Statistical significance was calculated using Student's t test. For association of *HMGCS2* with *UCP1*, Pearson's correlation coefficient was calculated. Statistical differences are indicated as *p < 0.05, **p < 0.01, ***p < 0.001.

2012). The relevance of human BAT in energy homeostasis is further supported by the association of its presence and activity with higher energy expenditure, lower adiposity, and reduced risk of insulin resistance (Chondronikola et al., 2014; Cypess et al., 2015; Iwen et al., 2017). BAT activation is therefore considered a promising strategy to increase energy expenditure and improve metabolic control. Unfortunately, the metabolic response of BAT to cold is blunted in obesity, and long-term administration of β_3-adrenoreceptor (β_3-AR) agonists might be associated with adverse side effects (Cypess et al., 2015; Orava et al., 2013). Hence, the identification of mechanisms driving brown adipocyte development and activity has been the focus of recent research. Here we show that protein geranylgeranylation plays an important role in the regulation of adipocyte browning, by modulating the activity of small GTPases. Our mouse and cell culture data are complemented by a retrospective clinical study and a small prospective trial supporting the physiological relevance of this regulation in humans.

RESULTS

HMGCS2 Is Enriched in Human BAT

To identify mechanisms regulating brown adipocyte function, we analyzed the transcriptome of human deep neck BAT and subcutaneous WAT biopsies. As expected, we found that uncoupling protein 1 (*UCP1*), along with other brown adipocyte marker genes, is highly enriched in BAT compared with WAT (Figures 1A and S1A). UCP1 was also enriched in human BAT at the protein level (Figures 1B and 1C). Interestingly, hydroxymethylglutaryl-coenzyme A (HMG-CoA) synthase 2 (*HMGCS2*) was one of the most highly enriched transcripts in human BAT (Figures 1A and S1A), in line with protein levels (Figures 1B and 1D). Furthermore, *HMGCS2* strongly correlated with *UCP1* expression (Figure 1E). These data could be confirmed in brown human multipotent adipose-derived stem (hMADS) cells, which exhibit an enrichment in HMGCS2, on both mRNA and protein levels (Figures 1F and 1G), along with an increase in expression of brown adipocyte marker genes (Figures 1F and S1B). Based on our data, we hypothesized that HMGCS2 might contribute to cellular HMG-CoA levels, which in turn could alter BAT activity.

Inhibition of HMG-CoA Synthesis Suppresses Brown Adipocyte Thermogenic Function

To study the role of HMG-CoA in the regulation of brown adipocyte function, we silenced both HMG-CoA synthase isoforms (Figure S1C). Knockdown of mitochondrial *Hmgcs2* in murine immortalized brown adipocytes (iBAs) and hMADS

cells led to a marked reduction of UCP1 mRNA and protein levels (Figures 2A, 2B, S2A, and S2B), along with a significant reduction of basal uncoupled and stimulated uncoupled mitochondrial respiration (Figures 2C and 2D). A similar inhibitory effect on UCP1 levels and uncoupled mitochondrial respiration was achieved by knockdown of the cytosolic *HMGCS1* (Figures 2A–2D, S2A, and S2B). Our results indicate that both HMG-CoA synthase isoforms are important for proper thermogenic brown adipocyte function. Interestingly, ketone body levels were not changed intracellularly nor in the supernatant between brown and white hMADS cells, and neither did we observe any effect of *HMGCS2* knockdown (Figure S2C), suggesting that the regulation of UCP1 upon knockdown of *HMGCS2* is independent of ketone body synthesis, but rather dependent on mevalonate. This is supported by the finding that mevalonate levels are higher in iBAT than in inguinal WAT (iWAT) of C57BL/6 mice (Figure S2D), suggesting the importance of the mevalonate pathway in brown adipocyte functionality.

Statins Inhibit Thermogenic Function of Adipocytes *In Vitro*

To confirm the significance of mevalonate in brown adipocyte physiology, we inhibited the mevalonate pathway using statins. At 1 μM concentration, only simvastatin and fluvastatin reduced UCP1 levels in iBAs (Figure 2E). However, all tested statins lowered UCP1 levels at 10 μM concentration (Figure 2F). Simvastatin showed an inhibitory effect already after 24 hr (Figure S2E). Unlike other statins, cerivastatin caused cell toxicity already at 1 μM concentration (Figure S2F). Interestingly, all tested statins inhibited preadipocyte proliferation without affecting brown adipocyte maturation (Figures S2G and S2H). Based on these results, we decided to use simvastatin in subsequent *in vitro* experiments, as it was shown to be more potent in inhibiting the mevalonate pathway in extrahepatic tissues than other statins (Olsson et al., 2002) and shows no toxic effect on mature adipocytes. Simvastatin dose dependently reduced UCP1 levels, as well as isoproterenol-stimulated uncoupled respiration in iBAs (Figures 2G, 2H, and S2I), which could be at least partially explained by reduced *Ucp1* promoter activity (Figure S2J). Importantly, also in hMADS cells, cerivastatin, simvastatin, and fluvastatin were more potent in reducing UCP1 levels than atorvastatin or rosuvastatin, without any signs of toxicity (Figures 2I and 2J). Interestingly, when mature white hMADS cells were exposed to rosiglitazone, to elicit the development of a brown phenotype (Elabd et al., 2009) in combination with simvastatin, a strong dose-dependent inhibitory effect of simvastatin on UCP1 was observed (Figures 2K and 2L). In addition, all tested statins inhibited phosphorylation of hormone-sensitive lipase (HSL) (Figures 2K and S2K). Altogether, these data indicate that the mevalonate pathway is important for the thermogenic function of brown and the browning of white adipocytes, *in vitro*.

Statins Inhibit iWAT Browning *In Vivo*

Next, we aimed to prove the importance of the mevalonate pathway in BAT function *in vivo*. Therefore, simvastatin and fluvastatin were administered to 12-week-old C57BL/6 mice by oral gavage at a dose of 10 mg/kg, which is equivalent to the dose used to treat hypercholesterolemia in patients (Nair and Jacob, 2016). Mice were exposed to statins for 2 days at 22°C to achieve inhibition of the mevalonate pathway, followed by 4 days of cold exposure, to induce thermogenesis (Figure 3A). Only fluvastatin reduced mevalonate levels in iBAT. However, both simvastatin and fluvastatin suppressed mevalonate production in iWAT (Figure S3A). Furthermore, geranyl pyrophosphate levels were decreased by both statins in iBAT and a trend toward reduction was observed also in iWAT, indicating that the mevalonate pathway was efficiently inhibited in both tissues (Figure S3B). We also quantified hydroxymethylglutaryl-coenzyme A reductase (HMGCR); however, statin administration had no effect on HMGCR expression in neither iBAT nor iWAT (Figures S3C–S3E). Similarly, HMGCR levels were not altered by statin treatment in hMADS cells, indicating that brown adipocytes do not respond to statins by HMGCR upregulation (Figure S3F). Interestingly, both statins inhibited browning of iWAT, without affecting UCP1 levels in iBAT (Figures 3B–3D). The inhibitory effect of statins on adipocyte browning was associated with higher iWAT and epididymal white adipose tissue (eWAT), but not iBAT mass (Figures 3E, 3F, and S3G). Fluvastatin had no effect on whole-body energy expenditure, metabolic rate, or food or water intake (Figures S3H–S3M). Based on these observations, we conclude that statins inhibit iWAT browning either directly by acting in mature adipocytes and/or precursor cells, or indirectly by affecting sympathetic nervous system (SNS) activity. Since brown adipocytes are activated already at room temperature (Kalinovich et al., 2017), we investigated the effect of statins in mice housed at thermoneutrality, to study whether the inhibitory effect of statins is mediated by reduced activity of the SNS. Therefore, 14-week-old C57BL/6 mice housed at 30°C were pretreated with fluvastatin for 2 days at a dose of 10 mg/kg, followed by 2 days of fluvastatin gavage combined with administration of CL-316.243 (0.1 mg/kg), a selective β_3-AR agonist to induce non-shivering thermogenesis (Figure 3G). Also in this experiment, fluvastatin reduced UCP1 levels in iWAT, despite a significant increase in CREB phosphorylation (Figures 3H and 3I). Similarly, brown adipocyte marker genes were significantly reduced in iWAT (Figure 3J), indicating suppression of adipocyte browning by fluvastatin. Brown adipocyte markers, UCP1 levels, and CREB phosphorylation were not affected by fluvastatin administration in iBAT (Figures S4A–S4C), suggesting that maximal activation of BAT might be able to overcome the inhibitory effect of statins. Fluvastatin-treated mice showed 2.1-fold higher iWAT mass (Figure 3K), indicating reduced lipid mobilization in response to the β_3-AR agonist. Importantly, by combining thermoneutrality with CL-316.243, we could show that the inhibitory effect of statins on iWAT browning is not mediated by reduced SNS activity, but rather is due to cell-autonomous effects.

Next, we employed *Ucp1*-CreERT2 × LoxP-Red mice, in which the number of recombined LoxP-Red sites reflects the amount of UCP1$^+$ cells within a given depot. Using this model (Figure S4D), we could show that fluvastatin treatment significantly reduced the number of UCP1$^+$ cells in iWAT, but not in iBAT (Figure 3L). Taken together, our results indicate that inhibition of the mevalonate pathway prevents adipocyte browning in mice *in vivo*.

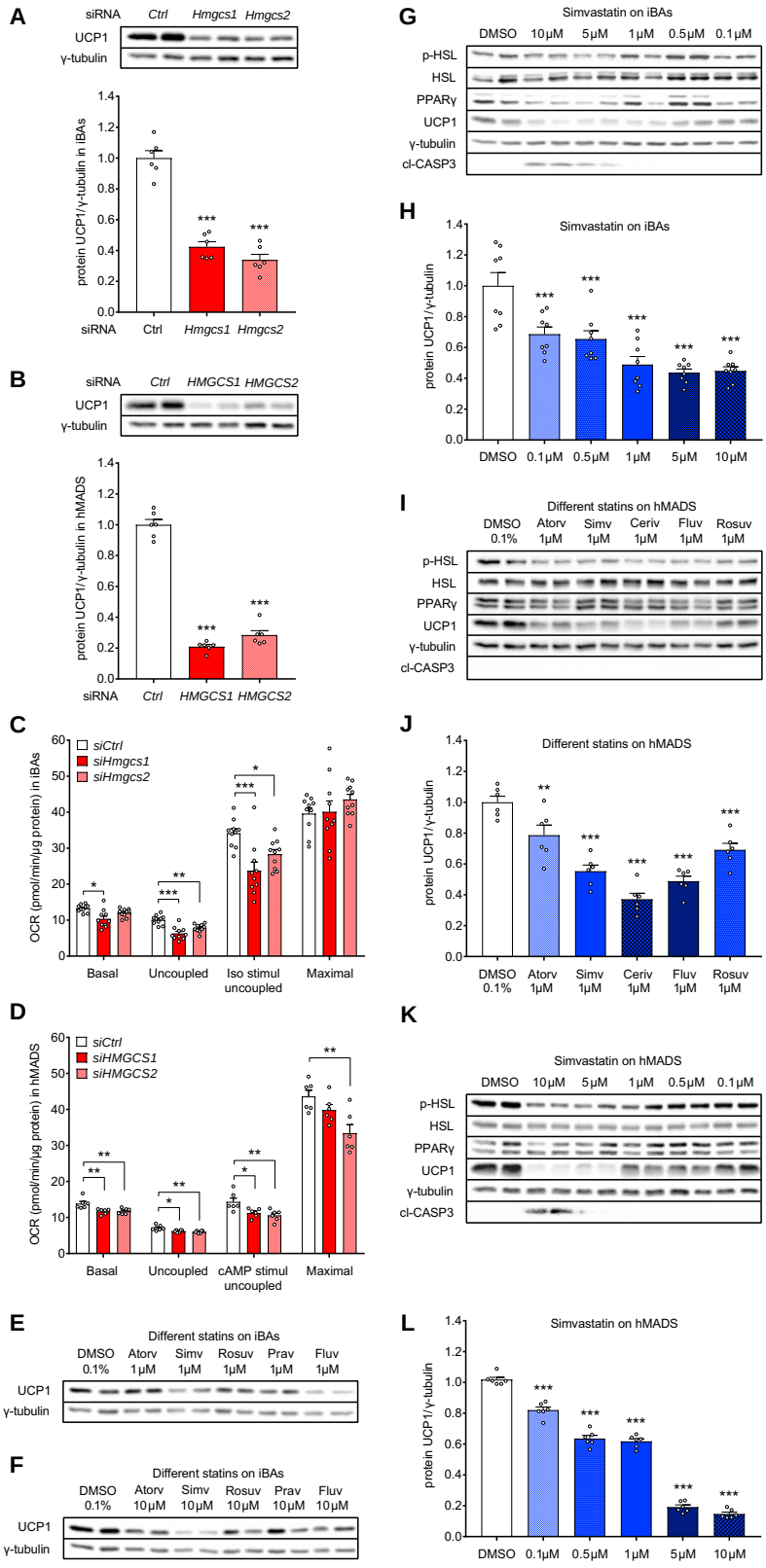

Figure 2. Inhibition of Mevalonate Pathway Suppresses Brown Adipocyte Thermogenic Function *In Vitro*

(A–D) Effect of *Hmgcs1* and *Hmgcs2* knockdown on UCP1 in (A) iBAs and (B) hMADS cells (n = 6). Effect of *Hmgcs1* and *Hmgcs2* knockdown on mitochondrial respiration in (C) iBAs (n = 10) and (D) hMADS cells (n = 6).

(E and F) Representative western blot (WB) showing effect of statin treatment (48 hr) on UCP1 in iBAs at (E) 1 μM and (F) 10 μM concentration (2 repeats).

(G and H) (G) Representative WB and (H) UCP1 quantification in iBAs treated (48 hr) with simvastatin (n = 8).

(I and J) (I) Representative WB and (J) UCP1 quantification in hMADS cells treated (48 hr) with different statins (n = 6).

(K and L) (K) Representative WB and (L) UCP1 quantification in hMADS cells treated (96 hr) with simvastatin (n = 6).

Results are reported as mean ± SEM. Statistical significance was calculated using ANOVA. Statistical differences are indicated as *$p < 0.05$, **$p < 0.01$, ***$p < 0.001$.

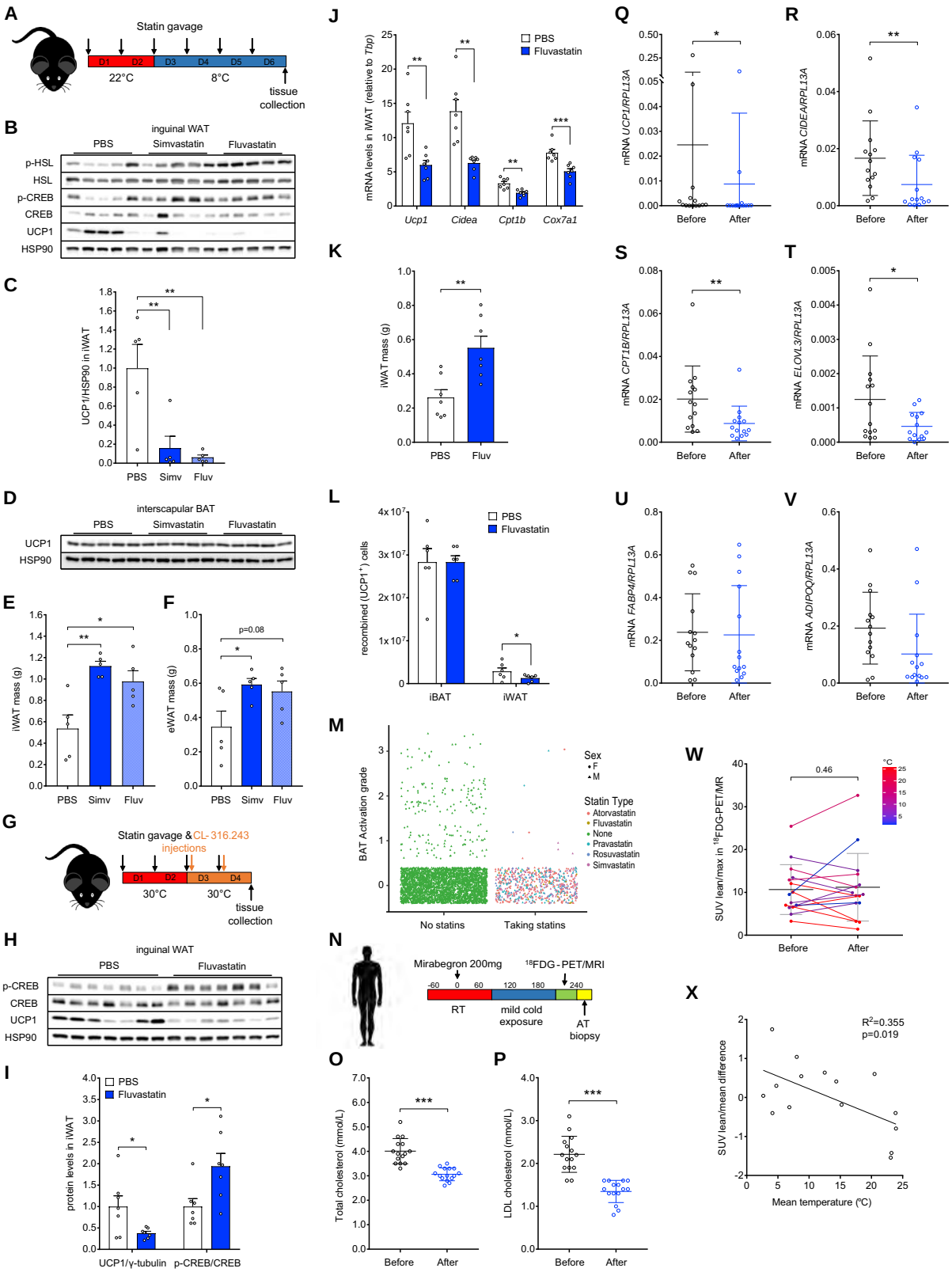

Figure 3. Statins Inhibit Adipose Tissue Browning in Mice and Men

(A) Schematic illustration of the *in vivo* statin treatment experiment.

(B–F) (B) Representative western blot (WB) and (C) UCP1 quantification in iWAT and (D) iBAT (n = 5). Effect of statins on (E) iWAT and (F) eWAT mass (n = 5).

(legend continued on next page)

Statin Use in Patients Is Inversely Associated with Active BAT

To investigate the effect of statins on BAT activity in humans, we conducted a retrospective study of all patients undergoing FDG-PET/CT at University Hospital of Zürich between November 2009 and February 2015. From a total of 8,409 patients, we identified 2,789 patients who had been hospitalized within 12 months prior to the PET/CT examination, for which we quantified BAT glucose uptake and analyzed statin use during the preceding hospitalization. From patients with multiple examinations (n = 738), the one with the strongest BAT activation was selected. Interestingly, we observed a significantly higher statin use among patients without active BAT (2,148 not on statins, 510 taking statins [19.2%]) compared with those with activated BAT (124 not on statins, 7 taking statins [5.3%]) (Figure 3M). Using a stepwise general linear regression with forward and backward feature selection, we found that statin use remained significantly associated with BAT inactivity after accounting for age, sex, and BMI (Table S1).

Statins Reduce Thermogenic Gene Expression in Human BAT

Next, we analyzed the effect of statins on activation of BAT in a prospective clinical trial. We performed the clinical trial with fluvastatin, which was more potent in inhibition of iWAT browning in our mouse experiments and shows higher systemic bioavailability and less interaction potential than other statins (Gazzerro et al., 2012). Furthermore, fluvastatin was the only statin in our retrospective study for which we did not identify any patient with active BAT (Figure 3M). We recruited 16 healthy young male lean volunteers with detectable BAT under stimulated conditions (Figure 3N). All participants underwent FDG-PET/MRI to confirm presence of active BAT, both before and after 14 days of fluvastatin treatment (80 mg/day). Two participants were excluded from the analysis due to non-compliance or failure of tissue sampling. In the 14 analyzed subjects, we could see a significant drop in total cholesterol and low-density lipoprotein (LDL) levels (Figures 3O and 3P). We could detect a significant reduction in expression of brown adipocyte markers *UCP1*, *CIDEA*, *CPT1B*, and *ELOVL3* (Figures 3Q–3T; Table S2), whereas general adipocyte markers such as *FABP4* and *ADIPOQ* were not changed by short-term fluvastatin therapy (Figures 3U and 3V). We did not detect any significant difference in expression of inflammatory markers (Figures S4E–S4G), with the exception of *TNFA*, which was slightly increased (Figure S4H). Expression of the glucose transporter *GLUT1* was not changed, whereas insulin-responsive *GLUT4* was significantly reduced following short-term fluvastatin treatment (Figures S4I and S4J). The inhibitory effect of statins on *GLUT4* expression has already been described in different cell types and tissues (Jiang et al., 2016; Li et al., 2016; Nakata et al., 2006). Short-term fluvastatin therapy had no effect on FDG uptake in the supraclavicular BAT depot (Figure 3W). Since the clinical trial spanned over 8 months, we included outside temperature, a known factor determining BAT activity, in the analysis (Cypess et al., 2009; Senn et al., 2018). Analysis of the data in relation to the outside temperature revealed a negative correlation between average temperature during the intervention and statin-induced changes in the average standardized uptake value normalized to lean body mass (SUVlean/mean) (Figure 3X), indicating that the effect of short-term fluvastatin therapy on glucose uptake might be temperature dependent or significantly smaller than the short-term effect of temperature alone. Furthermore, these data indicate that statins alter thermogenic gene expression in human BAT.

The Effects of Statins on UCP1 Are Mediated through Protein Prenylation

Next, we tested whether the negative effect of statins on UCP1 can be rescued by one of the downstream mevalonate intermediates. Interestingly, we could rescue the inhibitory effect of statin on *Ucp1* expression with mevalonate, farnesyl pyrophosphate (FPP), and geranylgeranyl pyrophosphate (GGPP), but not with squalene or coenzyme Q9 (Figure 4A). The rescue experiment was performed in the presence of exogenous cholesterol (10% fetal bovine serum [FBS]), suggesting that the effect of statins is not mediated by inhibition of cholesterol synthesis. The inhibitory effect of simvastatin on UCP1 levels could be observed also in FBS-free medium (Figures 2I–2L and S4K). In addition, the inhibitory effect of simvastatin could be completely rescued by geranylgeraniol (GGOH), the donor of a geranylgeranyl group (Figures 4B and 4C), but not by farnesol (FOH; Figures 4B and 4C), the donor of a farnesyl group, which unlike FPP does not serve as a direct precursor for GGPP synthesis. Similarly, we could also prevent the inhibitory effect of *Hmgcs1* knockdown on UCP1 levels in iBAs by GGPP (Figures S4L and S4M). Our data indicate that inhibition of the mevalonate pathway impairs UCP1 expression by blocking synthesis of FPP and GGPP, the substrates for protein prenylation. The inhibitory effect of statins on UCP1 expression and uncoupled mitochondrial respiration could be mimicked by GGTI-298 (Figures 4D–4F and S4N), a specific inhibitor of geranylgeranyltransferase I (GGTase I; Figure S1C), as well as by knockdown of the genes encoding the PGGT1B subunit of GGTase I and RABGGTB subunit of GGTase

(G) Schematic illustration of the *in vivo* fluvastatin treatment experiment.
(H and I) (H) Representative WB and (I) quantification of UCP1 and CREB phosphorylation (Ser133) in iWAT (n = 7).
(J and K) Effect of fluvastatin on (J) expression of brown adipocyte markers in iWAT and (K) iWAT mass (n = 7).
(L) Quantification of UCP1$^+$ cells in iBAT and iWAT of *Ucp1*-CreERT2 × LoxP-Red mice treated with fluvastatin (n = 6).
(M) Retrospective analysis of BAT activation grade in 2,789 patients shows a significantly higher number (chi-square test, p = 0.0001) of statin takers among patients without active BAT (19.2%) compared with patients with activated BAT (5.3%).
(N–W) (N) Schematic illustration of the clinical fluvastatin trial. Effect of fluvastatin therapy on (O) total cholesterol and (P) LDL levels (n = 15). Effect of short-term fluvastatin therapy on (Q) *UCP1*, (R) *CIDEA*, (S) *CPT1B*, (T) *ELOVL3*, (U) *FABP4*, and (V) *ADIPOQ* expression (n = 14) and (W) FDG uptake in supraclavicular BAT (n = 15). Different colors indicate average temperature during the fluvastatin intervention.
(X) Association of mean temperature during the fluvastatin intervention with change in SUVlean/mean in FDG-PET/magnetic resonance imaging (n = 15).
Results are reported as mean ± SEM for mouse experiments and mean ± SD for the clinical study. Statistical significance was calculated using ANOVA (B–F), Student's t test (H–P), and non-parametric Wilcoxon test (Q–W). Chi-square test was performed with R (m). For association of temperature and SUVlean/mean change, Pearson's correlation coefficient was calculated. Statistical differences are indicated as *p < 0.05, **p < 0.01, ***p < 0.001.

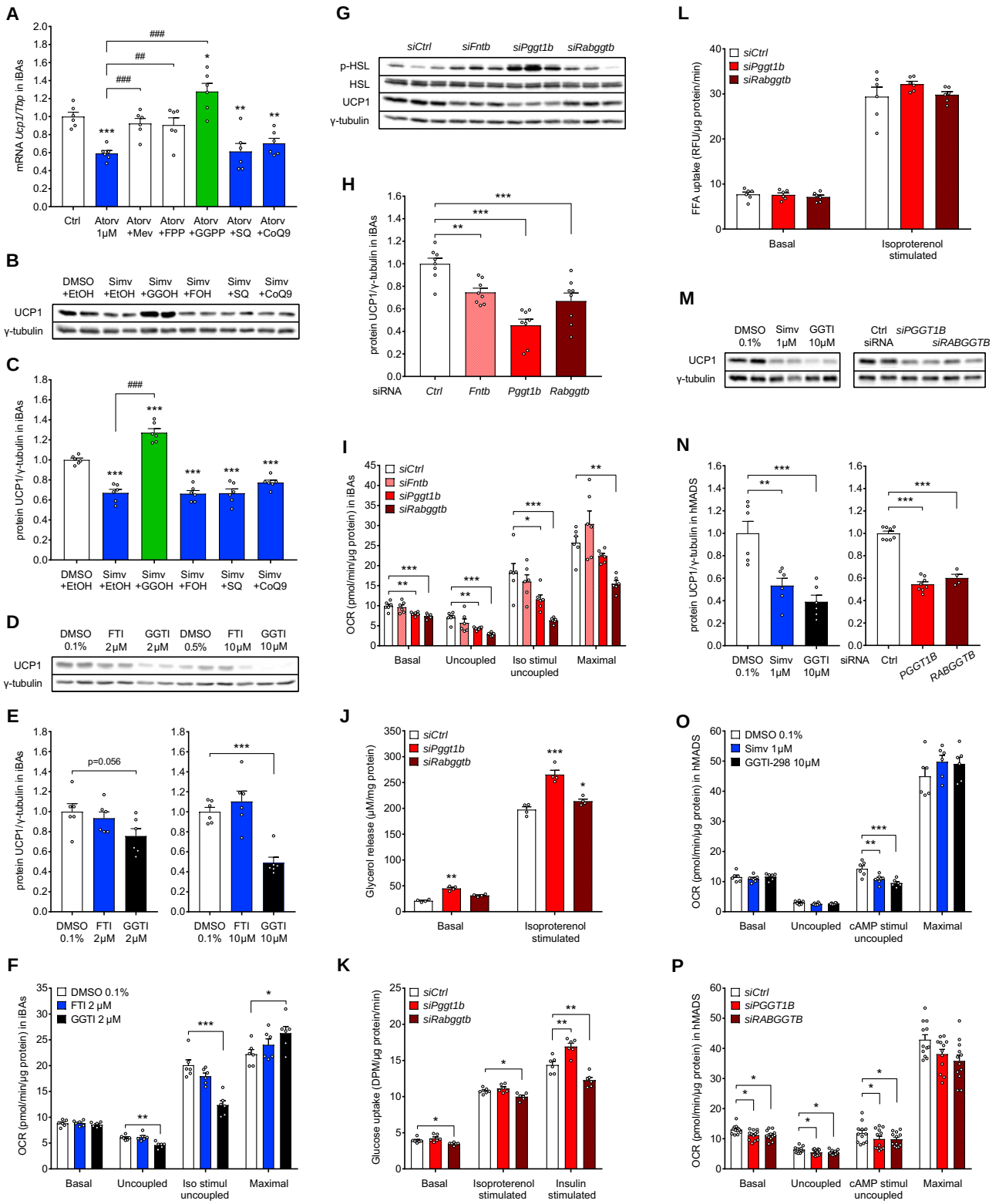

Figure 4. The Inhibitory Effect of Statins Can Be Rescued by GGPP

(A) The inhibitory effect of atorvastatin treatment (48 hr) on *Ucp1* expression in iBAs can be rescued by mevalonate (Mev; 500 μM), farnesyl pyrophosphate (FPP; 2 μM), and geranylgeranyl pyrophosphate (GGPP; 2 μM), but not by squalene (SQ; 10 μM) or coenzyme Q9 (CoQ9; 10 μM) (n = 6).

(B and C) (B) Representative WB and (C) quantification of the inhibitory effect of 1 μM simvastatin on UCP1 in iBAs, which can be rescued by GGOH (10 μM), but not by FOH (10 μM), SQ (10 μM), or CoQ9 (10 μM) (n = 6).

(legend continued on next page)

II (Figures 4G–4I and S4O) in iBAs. In contrast, the farnesyltransferase (FNTase) inhibitor FTI-277 as well as knockdown of the FNTB subunit of FNTase showed no effect on UCP1 levels and mitochondrial respiration (Figures 4D–4I, S4N, and S4O). Even the toxic effect of cerivastatin on mature iBAs could be prevented by FPP and GGPP (Figure S4P), but not by squalene or CoQ9. Knockdown of *Pggt1b* increased basal and isoproterenol-stimulated lipolysis but showed no effect on basal and isoproterenol-stimulated glucose and FFA uptake in iBAs (Figures 4J–4L). In contrast, knockdown of *Rabggtb* showed no or very little effect on lipolysis and FFA uptake, but significantly reduced glucose uptake in iBAs (Figures 4J–4L). To test the contribution of other mevalonate intermediates, we silenced the expression of key branching enzymes of this pathway. Knockdown of GGPP synthase (GGPS1), the enzyme providing substrate for protein geranylgeranylation, lowered UCP1 levels in iBAs (Figures S4Q and S4R). In contrast, knockdown of genes encoding the key enzymes of cholesterol and ubiquinone synthesis had no effect on UCP1 levels (Figures S4Q and S4R). Importantly, also in hMADS cells, GGTI-298 or knockdown of *PGGT1B* and *RABGGTB* reduced UCP1 levels and cAMP-stimulated uncoupled respiration (Figures 4M–4P). Altogether, our results indicate that the negative effect of mevalonate pathway inhibition on brown adipocyte activity and white adipocyte browning mainly results from depletion of GGPP.

GGTase I Regulates Adipocyte Browning *In Vivo*

Next, we tested whether the inhibitory effect of statin administration on browning of iWAT *in vivo* is mediated by inhibition of protein geranylgeranylation. Therefore, GGTI-298 was administered to 14-week-old male C57BL/6 mice by intraperitoneal injection at a dose of 1 mg/kg. The mice were kept for 2 days at 22°C to achieve inhibition of GGTase I, followed by acute cold exposure to induce thermogenesis (Figure S5A). GGTI-298 reduced UCP1 levels in iWAT (Figures 5A and 5B), confirming the important role of protein geranylgeranylation in the regulation of adipocyte browning. Next, we generated an inducible adipocyte-specific GGTase I (*Pggt1b*$^{fl/fl}$ × *Adip*-CreERT2) knockout mouse. Genetic deletion of GGTase I in mature adipocytes had no effect on UCP1 levels in iBAT (Figure S5B). However, UCP1 was significantly reduced in iWAT (Figures 5C and 5D), indicating suppression of adipocyte browning in response to β_3-AR agonist. Importantly, *Pggt1b* knockdown in mature adipocytes led to a slight decrease in energy expenditure, without affecting substrate preference, food and water intake, or ambulatory activity (Figures 5E and S5C–S5G). Injection of CL-316.243 increased the maximal energy expenditure and abrogated the effect of GGTase I deletion (Figure 5E). In addition, we found that GGTase I knockout mice, compared with the control littermates, gained more weight and developed impaired glucose tolerance when exposed to high-fat diet (Figures 5F–5H). Importantly, the effect on body weight and glucose tolerance could not be observed at thermoneutrality (Figures S5H–S5J), indicating that it results from reduction of non-shivering thermogenesis. Altogether, our data indicate that GGTase I activity is required for browning of iWAT *in vivo*.

GGPP Promotes Adipocyte Browning

Next, we tested whether protein prenylation can promote brown adipocyte activity. Treatment of mature iBAs with GGOH dose dependently increased UCP1 and mitochondrial respiration (Figures 5I–5K), whereas FOH had no effect on the thermogenic potential of iBAs (Figures S5K–S5M). Importantly, this effect of GGOH could be partially prevented by knockdown of *Pggt1b* and *Rabggtb* (Figures 5L and 5M). Interestingly, knockdown of both GGTases in parallel strongly reduced UCP1 levels in iBAs and completely blocked the stimulatory effect of GGOH (Figures 5N and 5O), indicating that the positive effect of GGOH on brown adipocyte activity is mediated by both GGTases. GGPP significantly increased UCP1 levels also in white hMADS cells (Figures 5P and 5Q), indicating that protein geranylgeranylation promotes adipocyte browning. This effect became apparent already after 48 hr (Figure S5N). Next, we tested the ability of GGOH to stimulate adipocyte browning *in vivo.* We treated 10-week-old C57BL/6 mice with GGOH at a dose of 50 mg/kg for 4 consecutive days. Even though GGOH had no significant effect on energy expenditure and UCP1 levels in iBAT (Figures S5O–S5Q), we observed a 3.5-fold induction of UCP1 in iWAT (Figures 5R and 5S), demonstrating that GGOH promotes adipocyte browning *in vivo.* In addition, the dose-dependent stimulatory effect of GGOH on UCP1 levels in iBAs was observed even upon knockdown of *Lxr*α, *Lxr*β, and *Ppar*γ (Figure S5R), suggesting that the positive effect of GGOH is independent of functional LXR and PPARγ signaling.

GGPP Is Required for the Prenylation of Small GTPases

To identify proteins undergoing geranylgeranylation, mature iBAs were first pretreated with simvastatin to block endogenous GGPP production and supplemented for 24 hr with regular or the azide form of GGOH. Proteins incorporating the GGOH-azide group were labeled using click chemistry. We detected a band of approximately 20 kDa, corresponding to the size of small GTPases, in both iBAs and hMADS cells (Figures 6A and 6B). Whereas in control cells small GTPases were predominantly located at the plasma membrane, inhibition of the mevalonate pathway led to a reduction of their membrane-bound levels

(D and E) (D) Representative western blot (WB) and (E) UCP1 quantification in iBAs treated for 48 hr with FTI-277 and GGTI-298 (n = 6).
(F) Effect of FTI-277 and GGTI-298 on mitochondrial respiration in iBAs (n = 6).
(G and H) (G) Representative WB and (H) UCP1 quantification in iBAs transfected with small interfering RNA (siRNA) pools targeting *Fntb*, *Pggt1b*, and *Rabggtb* (n = 8).
(I–L) (I) Effect of prenyl-transferase knockdown on mitochondrial respiration in iBAs (n = 6). Effect of GGTase knockdown on (J) glycerol release (n = 4), (K) glucose (n = 6), and (L) free fatty acid uptake (n = 6) in iBAs.
(M and N) (M) Representative WB and (N) UCP1 quantification in hMADS cells treated with simvastatin or GGTI-298 (n = 6) or transfected with the siRNA pools targeting *PGGT1B* (n = 8) or *RABGGTB* (n = 4).
(O and P) (O) Effects of GGTI-298 and simvastatin (n = 6) and (P) *PGGT1B* and *RABGGTB* knockdown on mitochondrial respiration in hMADS cells (n = 12).
Results are reported as mean ± SEM. Statistical significance was calculated using ANOVA and Student's t test. Statistical differences are indicated as $^{*}p < 0.05$, $^{**}p < 0.01$, $^{***}p < 0.001$; and $^{\#\#}p < 0.01$, $^{\#\#\#}p < 0.001$.

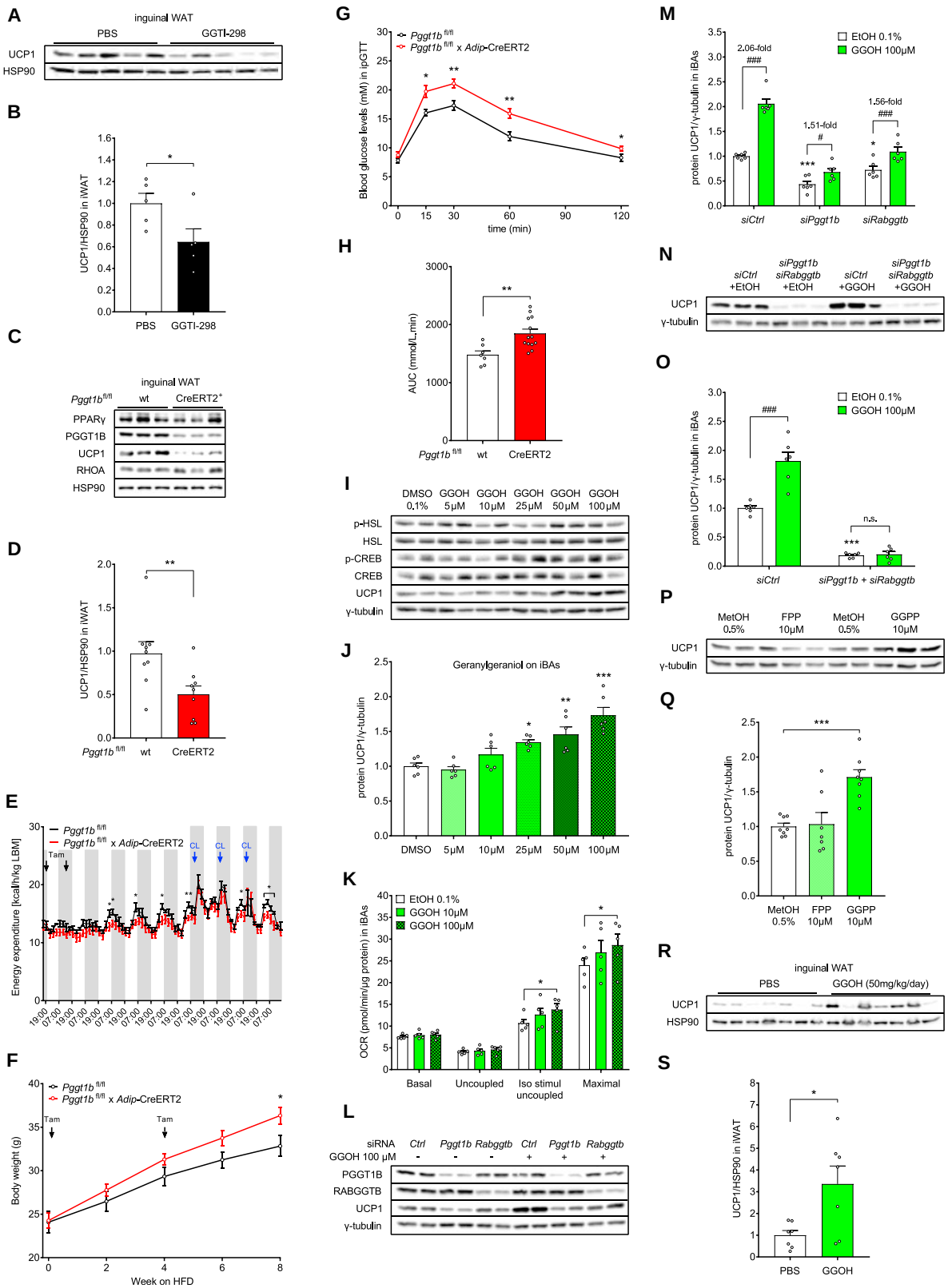

Figure 5. GGOH Promotes Adipocyte Browning *In Vitro* as well as *In Vivo*

(A and B) (A) Representative western blot (WB) and (B) UCP1 quantification in iWAT of C57BL/6 mice treated with PBS and GGTI-298 for 6 days (1 mg/kg; n = 5). (C and D) (C) Representative WB and (D) UCP1 quantification in iWAT of control (*Pggt1b*$^{fl/fl}$) and *Pggt1b*$^{fl/fl}$ × *Adip*-CreERT2 mice (n = 9).

(legend continued on next page)

and an increase of their cytosolic levels (Figures 6C–6F), indicating impairment of small GTPase geranylgeranylation. A similar shift in subcellular distribution was achieved by GGTI-298 and fluvastatin (Figures 6C–6F, S6A, and S6B). This effect of statins could be completely prevented by GGOH (Figure S6C). Cellular RHOA levels increased in response to statins, in both iBAs and hMADS cells (Figures 6G–6I and S6D), which could be a compensation for reduced RHO signaling. The effect of statins could be completely rescued by GGOH, but not by FOH, squalene, or CoQ9 (Figure 6G). Interestingly, Gallein, a specific inhibitor of the γ subunit of G protein, had no effect on UCP1 and RHOA levels in iBAs or browning of hMADS cells (Figures S6E–S6G), suggesting that the inhibitory effect of statins most likely does not result from impaired G-protein prenylation. In contrast, inhibition of RHO family members with the aid of Rhosin reduced UCP1 and cAMP-stimulated uncoupled respiration in hMADS cells (Figures 6J–6L), indicating that small GTPases might be important for adipocyte browning.

Small GTP-Binding Proteins Are Important for Adipocyte Browning

Next, we silenced the five most common small GTPases, which are abundantly expressed in adipocytes and require the C-terminal geranylgeranyl group for proper function. Knockdown of *Rhoa*, *Rhob*, *Cdc42*, *Rap1a*, and *Rap1b* affected UCP1 levels in iBAs, as well as UCP1 levels and mitochondrial respiration in hMADS cells (Figures 7A–7E). Moreover, the stimulatory effect of GGOH on UCP1 in iBAs could be partially suppressed by knockdown of individual small GTPases (Figures 7F and 7G). Several small GTP-binding proteins were shown to participate in the regulation of the cellular cytoskeleton. In agreement with our hypothesis, simvastatin dose dependently reduced F-actin levels in iBAs (Figure 7H). Importantly, this effect of simvastatin could also be prevented by GGOH in both cell lines (Figure 7I), indicating that the effect of mevalonate pathway inhibitors might be, at least partially, explained by regulation of the actin cytoskeleton. In many different cell types, it was shown that cellular F-actin levels determine the activity of the transcriptional co-regulators YAP1 and TAZ (Aragona et al., 2013). In line with our previous observations, levels of YAP1 and TAZ in iBAs were strongly reduced following simvastatin treatment (Figures 7J and 7K) and also this effect could be prevented by GGOH, which strongly increased the levels of these transcriptional co-regulators (Figure 7K). Similarly, knockdown of *PGGT1B*, but not *RABGGTB*, significantly reduced levels of YAP1 and TAZ in hMADS cells (Figures 7L and 7M). Furthermore, knockdown of YAP1 and TAZ led to a significant reduction of UCP1 and uncoupled mitochondrial respiration in hMADS cells (Figures 7N–7P), indicating that these transcriptional co-regulators are important for adipocyte browning. Taken together, our data indicate that small GTPases play an important role in regulation of the thermogenic function of brown adipocytes and white adipocyte browning, and their activity requires the availability of GGPP, the substrate for protein geranylgeranylation.

DISCUSSION

Several studies in recent years have shown that activation of BAT can promote energy expenditure and thus protect from the development of metabolic disease (Hanssen et al., 2015). We and others (Svensson et al., 2011) have identified *HMGCS2* as one of the most highly enriched transcripts in human BAT. HMGCS2 has been implicated in the synthesis of ketone bodies, and recent work has suggested that ketone bodies can regulate adipocyte browning (Carriere et al., 2014); however, based on our data, it seems that the negative effect of HMGCS2 knockdown on thermogenic function and adipocyte browning is not mediated through ketone bodies. We therefore speculate that HMGCS2 might rather contribute to cellular HMG-CoA levels and thereby provide substrate for mevalonate synthesis. Indeed, it was shown that transfection of *Hmgcs2* cDNA was able to restore cholesterol synthesis in HMGCS1-deficient CHO-K1 cells (Ortiz et al., 1994). The role of the mevalonate pathway in regulation of BAT function is further supported by studies showing cold-induced increase in *Hmgcs1* expression in both iWAT and iBAT (Forner et al., 2009; Shore et al., 2013). In line with these observations, we could show that mevalonate levels are higher in iBAT than in iWAT. We believe that the flux through the mevalonate pathway is determined mainly by the availability of HMG-CoA, the substrate for mevalonate synthesis.

We show here that inhibition of the mevalonate pathway affects uncoupling in mature human and murine brown adipocytes, and in line with these findings we observed a reduced uncoupled mitochondrial respiration *in vitro*. Pharmacological inhibition of the mevalonate pathway using statins showed no significant effect on UCP1 levels in iBAT, whereas browning of the iWAT was significantly reduced. Statins did not change the energy expenditure, possibly because the maximal capacity for iBAT activation was not affected, while it primarily affected the activity of brite cells in iWAT. This is in line with the recent findings demonstrating that the main thermogenic capacity in mice is present in brown and not in brite adipocytes (Kalinovich et al., 2017), and fits with

(E) Effect of *Pggt1b* deletion on energy expenditure (wild-type n = 4; CreERT2 n = 7).
(F–H) (F) Body weight gain and (G and H) glucose tolerance in *Pggt1b* $^{fl/fl}$ × *Adip*-CreERT2 mice (n = 13) and control littermates (n = 7) after 8 weeks on high-fat diet.
(I–K) (I) Representative WB, (J) UCP1 quantification (n = 6), and (K) mitochondrial respiration (n = 5) in iBAs treated for 48 hr with GGOH.
(L and M) (L) Representative WB and (M) UCP1 quantification in iBAs transfected with small interfering RNA (siRNA) pools targeting individual geranylgeranyltransferases in combination with GGOH treatment (48 hr; n = 6).
(N and O) (N) Representative WB and (O) UCP1 quantification in iBAs transfected with siRNA pools targeting both GGTases in combination with GGOH treatment (48 hr; n = 6).
(P and Q) (P) Representative WB and (Q) UCP1 quantification in white hMADS cells treated (96 hr) with FPP, GGPP, or methanol (control; 0.5%) (n = 8).
(R and S) (R) Representative WB and (S) UCP1 quantification in iWAT of C57BL/6 mice treated with PBS or GGOH for 4 consecutive days (n = 7). Tam, tamoxifen administration.
Results are reported as mean ± SEM. Statistical significance was calculated using ANOVA and Student's t test. Statistical differences are indicated as $^{*}p < 0.05$, $^{**}p < 0.01$, $^{***}p < 0.001$; and $^{\#}p < 0.05$, $^{\#\#\#}p < 0.001$.

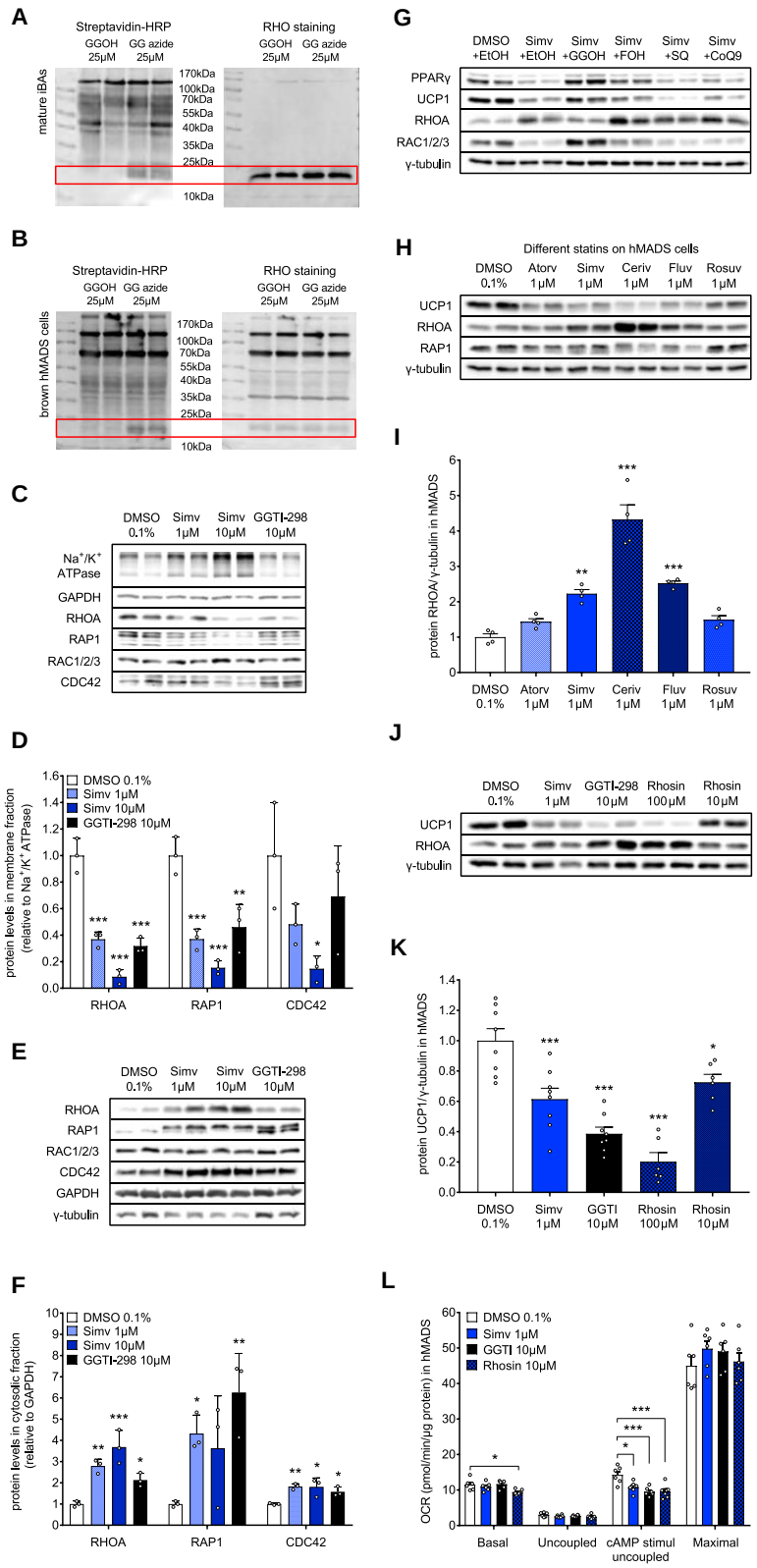

Figure 6. Inhibition of the Mevalonate Pathway Impairs Geranylgeranylation of Small GTP-Binding Proteins

(A–F) Representative western blot (WB) showing incorporation of GGOH azide (A) in iBAs and (B) in hMADS cells (n = 2; 3 repeats). Representative WB and quantification, respectively, of RHOA, RAP1, RAC1/2/3, and CDC42 in (C and D) membrane and (E and F) cytosolic fraction of iBAs treated with simvastatin or GGTI-298 for 48 hr (n = 3; 3 repeats).

(G–K) (G) Representative WB showing increase of RHOA in iBAs in response to simvastatin treatment (48 hr), which could be prevented by GGOH (100 μM), but not by FOH (100 μM), SQ (10 μM), or CoQ9 (10 μM) (2 repeats). Representative WB and quantification, respectively, of UCP1 and RHOA in hMADS cells treated with (H and I) different statins (n = 4) or (J and K) GGTI-298 and Rhosin for 96 hr (n = 6–8).

(L) Effect of simvastatin, GGTI-298, and Rhosin treatment (96 hr) on mitochondrial oxygen consumption rate (OCR) in hMADS cells (n = 6). Results are reported as mean ± SEM. Statistical significance was calculated using ANOVA and Student's t test. Statistical differences are indicated as *p < 0.05, **p < 0.01, ***p < 0.001.

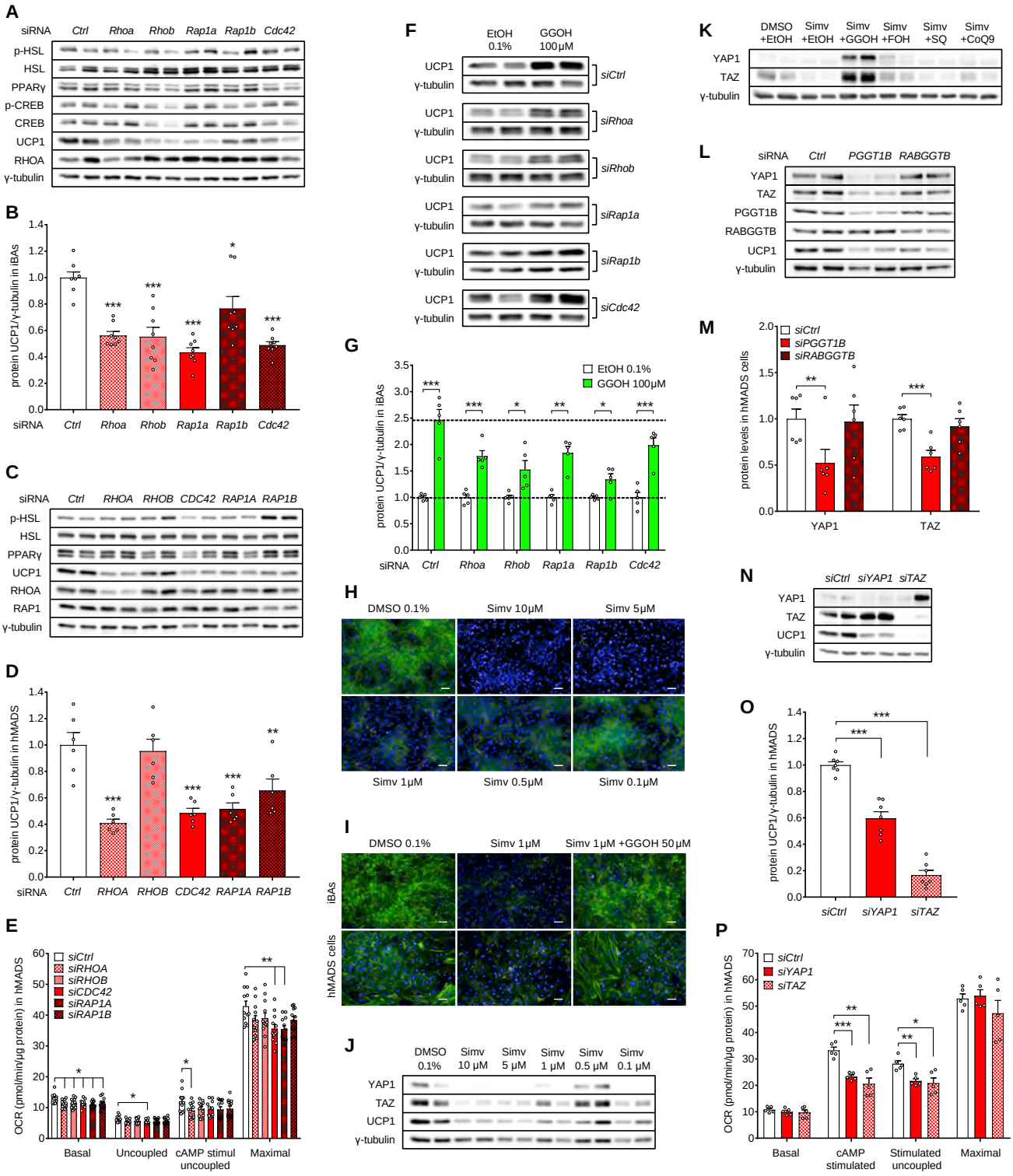

Figure 7. Small GTP-Binding Proteins Are Important for Adipocyte Thermogenic Function

(A and B) (A) Representative western blot (WB) and (B) UCP1 quantification in iBAs transfected with siRNA pools targeting individual small GTPases (n = 7–8).

(C and D) (C) Representative WB and (D) UCP1 quantification in hMADS cells transfected with siRNA pools targeting individual small GTPases (n = 6).

(E) Effect of individual small GTPase knockdown on mitochondrial respiration in hMADS cells (n = 12).

(F and G) (F) Representative WB and (G) UCP1 quantification in iBAs transfected with siRNA pools targeting individual small GTPases in combination with GGOH treatment (48 hr; n = 5).

(H) Effect of simvastatin treatment (48 hr) on F-actin levels in iBAs (F-actin in green, nuclei in blue). Scale bar, 50 µm.

(legend continued on next page)

findings of several studies, which did not observe changes in energy expenditure upon statin treatment (Chung et al., 2008; Panayiotou et al., 2013). It is important, however, to point out that we used statins as a pharmacological tool to achieve short-term inhibition of the mevalonate pathway. Statins are normally taken over several decades and long-term changes in brite adipocyte content might have a significant impact on whole-body metabolism. In addition, it should be noted that statins have many positive effects in different tissues, which makes it very complicated to dissect the impact of beige fat inhibition on whole-body metabolism in such a model. Therefore, we used the much more defined inducible adipocyte-specific ablation of GGTase I, which led to inhibition of iWAT browning, development of obesity, and impaired glucose tolerance after 8 weeks on a high-fat diet. Moreover, this negative metabolic phenotype did not develop at thermoneutrality, demonstrating that it results from impaired adipose tissue thermogenesis. This is in line with multiple reports indicating that regulating brite adipocyte formation is sufficient to elicit a metabolic phenotype (Cohen et al., 2014; Kazak et al., 2015; Qiang et al., 2012; Shinoda et al., 2015).

In adult humans, BAT depots seem to contain both classical and inducible brown adipocytes (Jespersen et al., 2013; Lidell et al., 2013). Interestingly, we found an inverse correlation of statin use with active BAT in a retrospective study. In the prospective clinical trial, we found that fluvastatin could reduce expression of brown adipocyte markers in supraclavicular BAT; however, no significant effect on FDG uptake was observed. Based on the current literature, FDG-PET is the most widely used technique to measure BAT presence in humans because of difficulties in tissue sampling and/or the measurement of whole-body energy expenditure using indirect calorimetry. As several groups have shown that *Ucp1*-knockout mice exhibit the same levels of radiolabeled glucose uptake in BAT as wild-type mice (Hankir et al., 2017; Olsen et al., 2017), it is difficult to assess whether FDG is the ideal measure for BAT activity given the wide substrate use of this tissue. Interestingly, the changes in BAT glucose uptake induced by fluvastatin treatment seem to be temperature dependent, suggesting that thermogenesis and glucose uptake are coupled only under partially stimulated conditions. Further studies will be needed to expand these results.

Several papers have reported that atorvastatin treatment inhibits preadipocyte proliferation and adipogenic differentiation, without affecting adipocyte maturation (Li et al., 2003). This is in line with reports showing that statins reduce PPARγ, C/EBPα, and C/EBPβ levels (Mauser et al., 2007; Nakata et al., 2006). We exclusively investigated here the role of the mevalonate pathway in mature brown adipocytes and in the conversion of white into brown adipocytes, and we could show that statins reduce thermogenic function and PPARγ levels, without affecting the number of differentiated cells. We have recently shown that PPARγ is required to maintain the thermogenic capacity of mature brown adipocytes (Lasar et al., 2018); thus it is possible that statins inhibit BAT function through regulation of this factor.

The inhibitory effect of statins on UCP1 levels in brown adipocytes *in vitro* could be rescued by GGPP, FPP, and GGOH, but not by FOH. Metabolic labeling experiments have provided evidence that mammalian cells can use free GGOH for protein geranylgeranylation and free FOH for sterol biosynthesis and protein farnesylation (Crick et al., 1994; Fliesler and Keller, 1995). However, there is very little evidence for the conversion of FOH back to FPP and GGPP and it is mostly based on studies from plants (Thai et al., 1999). Another point of evidence against the conversion of FOH to FPP is based on multiple studies investigating the inhibitory effect of statins on the proliferation of smooth muscle, NIH 3T3, and C6 glioma cells, which could be rescued by GGPP or GGOH, but not by FOH (Crick et al., 1998; Vigano et al., 1995; Vogt et al., 1996). On the other hand, one study showed increased FPP production in rat liver lysates following FOH supplementation (Bentinger et al., 1998). The authors of this study suggest that an enzyme phosphorylating FOH into farnesyl monophosphate, as well as an enzymatic mechanism catalyzing the phosphorylation of farnesyl-P to farnesyl-PP, exists. However, these enzymes have not been identified as of yet.

Based on our data we conclude that the development and thermogenic function of brite but not of classical brown adipocytes are affected by inhibition of the mevalonate pathway and prenylation of small GTPases. We quantified not only the expression of thermogenic markers, but also the number of UCP1$^+$ cells, which are significantly reduced by statins in the iWAT. Therefore, we believe that the mevalonate pathway and particularly protein prenylation are important for iWAT browning, but do not affect the thermogenic potential of fully active BAT. Nevertheless, we cannot rule out that the effect of the mevalonate pathway and GGTase I inhibition on adipocyte browning in mice is in part due to changes in brite adipocyte formation from precursors (Wang and Scherer, 2014). An argument against such a contribution stems from our genetic model, as we could show that ablation of GGTase I exclusively in mature adipocytes led to a similar effect observed in statin- and GGTI-298-treated mice. These data indicate that the effect occurs at the level of maturation or interconversion, rather than through changes in adipogenesis. Another support for this argument is the fact that mature adipocytes do not de-differentiate upon statin treatment or inhibition of protein geranylgeranylation.

We propose that the activity of the mevalonate pathway regulates adipocyte browning by affecting geranylgeranylation of small GTP-binding proteins. It has been shown recently that expression of constitutively active G_q protein reduces brown adipogenesis in mice via modulation of RHOA/ROCK signaling (Klepac et al., 2016). In addition, the pro-adipogenic effect of

(I) Effect of simvastatin treatment on F-actin levels in iBAs and hMADS cells (F-actin in green, nuclei in blue) can be rescued with GGOH. Scale bar, 50 μm.
(J and K) (J) Representative WB showing dose-dependent inhibitory effect of simvastatin treatment (48 hr) on YAP1 and TAZ levels in iBAs, which (K) could be rescued with GGOH (100 μM).
(L and M) (L) Representative WB and (M) YAP1 and TAZ quantification in hMADS cells transfected with siRNA pools targeting *PGGT1B* and *RABGGTB* (n = 6).
(N and O) (N) Representative WB and (O) UCP1 quantification in hMADS cells transfected with siRNA pools targeting *YAP1* and *TAZ* (n = 7).
(P) Effect of *YAP1* and *TAZ* knockdown on mitochondrial respiration in hMADS cells (n = 5).
Results are reported as mean ± SEM. Statistical significance was calculated using ANOVA and Student's t test. Statistical differences are indicated as $^*p < 0.05$, $^{**}p < 0.01$, $^{***}p < 0.001$.

BMP7 is mediated by suppression of ROCK activity; however, ROCK inhibition does not alter BMP7-induced UCP1 expression in C3H/10T1/2 mesenchymal stem cells differentiated into brown adipocytes (McDonald et al., 2015). In a proof-of-principle experiment, knockdown of the five most common GTPases resulted in a significant reduction of UCP1 levels, indicating that members of this protein class are important for function and/or formation of thermogenic adipocytes. Based on our data it seems that small GTPases have overlapping functions in the regulation of UCP1, and the effect of protein geranylgeranylation is most likely mediated by multiple pathways and not by a single target. We believe that, similar to GGTase I inhibition, GGTase II knockdown also affects many cellular processes, including vesicular transport, in which RAB proteins play a crucial role. One of the mechanisms for how impaired geranylgeranylation of small GTP-binding proteins might affect thermogenic function and adipocyte browning is impairment of F-actin formation and transcriptional activity of YAP1 and TAZ. This is supported by a recent study showing the importance of actomyosin tension and the mechanosensitive transcriptional co-activators YAP1 and TAZ for induction of oxidative metabolism and uncoupled respiration in thermogenic fat cells (Tharp et al., 2018).

In conclusion, we show that the mevalonate pathway regulates adipocyte browning. Our mouse and cell culture data are supported in part by a retrospective and a small prospective volunteer study, supporting the physiological relevance of this regulation in humans. Further clinical studies are warranted to substantiate these results and to determine whether protein geranylgeranylation or individual small GTPases might be used for therapeutic strategies to promote thermogenic activity of fat cells and thereby increase whole-body energy expenditure.

Limitations of Study

Retrospective data presented in our study should be interpreted with caution, as retrospective studies suffer from numerous weaknesses, most notably a selection bias. This may be particularly true in our cohort of mostly cancer patients, which are probably not representative of the general population. Our small prospective volunteer study shows that short-term fluvastatin treatment reduces expression of brown adipocyte markers without affecting FDG uptake in supraclavicular BAT. Further studies will be needed to test the effect of other statins on BAT activity in large patient cohorts. We provide a possible explanation for reduced UCP1 levels, namely impaired geranylgeranylation of small GTPases, which then leads to reduced F-actin levels and YAP1/TAZ inactivity. However, it is important to mention that small GTPases are involved in the regulation of a large variety of processes, and the inhibitory effect on adipocyte browning can, most likely, not be explained solely by dysregulation of YAP1 and TAZ. Further studies will be needed to completely dissect the mechanism downstream of GGTases.

STAR★METHODS

Detailed methods are provided in the online version of this paper and include the following:

- KEY RESOURCES TABLE
- CONTACT FOR REAGENT AND RESOURCE SHARING
- EXPERIMENTAL MODEL AND SUBJECT DETAILS
  - Clinical Transcriptome Study
  - Retrospective ^{18}FDG-PET/CT Cohort Study
  - Clinical Fluvastatin Study
  - Mouse Experiments
  - Cell Culture – hMADS Cells
  - Cell Culture – Immortalized Murine Brown Adipocytes
- METHOD DETAILS
  - Intraperitoneal Glucose Tolerance Test
  - Body Composition Measurement
  - Indirect Calorimetry
  - Tissue Harvest
  - Analysis of Preadipocyte Proliferation and Adipocyte Differentiation
  - Cellular Respiration
  - Fatty Acid Uptake
  - Lipolysis
  - Glucose Uptake
  - Ketone Bodies Measurement
  - *Ucp1* Promoter Activity
  - RNA Extraction, cDNA Synthesis, Quantitative RT-PCR
  - Protein Extraction and Western Blot
  - Click Chemistry
  - Subcellular Fractionation
  - F-actin Staining
  - RNA Sequencing, Mapping and Analysis
  - Quantification of Cre Recombination in Mouse Tissues
  - Metabolomic Analysis
- QUANTIFICATION AND STATISTICAL ANALYSIS
- DATA AND SOFTWARE AVAILABILITY

SUPPLEMENTAL INFORMATION

Supplemental Information includes seven figures and four tables and can be found with this article online at https://doi.org/10.1016/j.cmet.2018.11.017.

ACKNOWLEDGMENTS

The work was supported by the International Starr Foundation, the Vontobel-Stiftung, the Swiss National Science Foundation, and the Grant Agency of the Slovak Academy of Sciences (VEGA 2/0096/17).

AUTHOR CONTRIBUTIONS

M. Balaz and C.W. designed the study; M. Balaz, I.A.B., M.J.B., L.V., and C.W. supervised the experiments; M. Balaz, L.B., L.S., W.S., H.D., C.M., C.H., Y.R., S.M., and V.E. performed the experiments; M. Balaz, J.U., L.V., P.S., B.U., and M.P. performed the clinical transcriptome study; L.O. analyzed RNA sequencing data; A.S.B., S.B., C.Z., and C.F. performed the retrospective clinical study; A.S.B., J.M., G.G., C.I.M., I.A.B., and M.J.B. performed the clinical trial; N.Z. performed the metabolome analysis; M. Bergo, M.K.A., and E.-Z.A. provided resources; M. Balaz, A.S.B., and C.W. wrote the paper; all authors reviewed and edited the manuscript.

DECLARATION OF INTERESTS

The authors declare no competing interests.

Received: August 14, 2018
Revised: October 15, 2018
Accepted: November 27, 2018
Published: December 20, 2018

REFERENCES

Aragona, M., Panciera, T., Manfrin, A., Giulitti, S., Michielin, F., Elvassore, N., Dupont, S., and Piccolo, S. (2013). A mechanical checkpoint controls multicellular growth through YAP/TAZ regulation by actin-processing factors. Cell *154*, 1047–1059.

Bartelt, A., Bruns, O.T., Reimer, R., Hohenberg, H., Ittrich, H., Peldschus, K., Kaul, M.G., Tromsdorf, U.I., Weller, H., Waurisch, C., et al. (2011). Brown adipose tissue activity controls triglyceride clearance. Nat. Med. *17*, 200–205.

Becker, A.S., Nagel, H.W., Wolfrum, C., and Burger, I.A. (2016). Anatomical grading for metabolic activity of brown adipose tissue. PLoS One *11*, e0149458.

Bentinger, M., Grunler, J., Peterson, E., Swiezewska, E., and Dallner, G. (1998). Phosphorylation of farnesol in rat liver microsomes: properties of farnesol kinase and farnesyl phosphate kinase. Arch. Biochem. Biophys. *353*, 191–198.

Cannon, B., and Nedergaard, J. (2004). Brown adipose tissue: function and physiological significance. Physiol. Rev. *84*, 277–359.

Carriere, A., Jeanson, Y., Berger-Muller, S., Andre, M., Chenouard, V., Arnaud, E., Barreau, C., Walther, R., Galinier, A., Wdziekonski, B., et al. (2014). Browning of white adipose cells by intermediate metabolites: an adaptive mechanism to alleviate redox pressure. Diabetes *63*, 3253–3265.

Chondronikola, M., Volpi, E., Borsheim, E., Porter, C., Annamalai, P., Enerback, S., Lidell, M.E., Saraf, M.K., Labbe, S.M., Hurren, N.M., et al. (2014). Brown adipose tissue improves whole-body glucose homeostasis and insulin sensitivity in humans. Diabetes *63*, 4089–4099.

Chung, J., Brass, E.P., Ulrich, R.G., and Hiatt, W.R. (2008). Effect of atorvastatin on energy expenditure and skeletal muscle oxidative metabolism at rest and during exercise. Clin. Pharmacol. Ther. *83*, 243–250.

Cohen, P., Levy, J.D., Zhang, Y., Frontini, A., Kolodin, D.P., Svensson, K.J., Lo, J.C., Zeng, X., Ye, L., Khandekar, M.J., et al. (2014). Ablation of PRDM16 and beige adipose causes metabolic dysfunction and a subcutaneous to visceral fat switch. Cell *156*, 304–316.

Crick, D.C., Andres, D.A., Danesi, R., Macchia, M., and Waechter, C.J. (1998). Geranylgeraniol overcomes the block of cell proliferation by lovastatin in C6 glioma cells. J. Neurochem. *70*, 2397–2405.

Crick, D.C., Waechter, C.J., and Andres, D.A. (1994). Utilization of geranylgeraniol for protein isoprenylation in C6 glial cells. Biochem. Biophys. Res. Commun. *205*, 955–961.

Cypess, A.M., Lehman, S., Williams, G., Tal, I., Rodman, D., Goldfine, A.B., Kuo, F.C., Palmer, E.L., Tseng, Y.H., Doria, A., et al. (2009). Identification and importance of brown adipose tissue in adult humans. N. Engl. J. Med. *360*, 1509–1517.

Cypess, A.M., Weiner, L.S., Roberts-Toler, C., Franquet Elia, E., Kessler, S.H., Kahn, P.A., English, J., Chatman, K., Trauger, S.A., Doria, A., et al. (2015). Activation of human brown adipose tissue by a beta3-adrenergic receptor agonist. Cell Metab. *21*, 33–38.

Elabd, C., Chiellini, C., Carmona, M., Galitzky, J., Cochet, O., Petersen, R., Penicaud, L., Kristiansen, K., Bouloumie, A., Casteilla, L., et al. (2009). Human multipotent adipose-derived stem cells differentiate into functional brown adipocytes. Stem Cells *27*, 2753–2760.

Fliesler, S.J., and Keller, R.K. (1995). Metabolism of [3H]farnesol to cholesterol and cholesterogenic intermediates in the living rat eye. Biochem. Biophys. Res. Commun. *210*, 695–702.

Forner, F., Kumar, C., Luber, C.A., Fromme, T., Klingenspor, M., and Mann, M. (2009). Proteome differences between brown and white fat mitochondria reveal specialized metabolic functions. Cell Metab. *10*, 324–335.

Frontini, A., Vitali, A., Perugini, J., Murano, I., Romiti, C., Ricquier, D., Guerrieri, M., and Cinti, S. (2013). White-to-brown transdifferentiation of omental adipocytes in patients affected by pheochromocytoma. Biochim. Biophys. Acta *1831*, 950–959.

Fuhrer, T., Heer, D., Begemann, B., and Zamboni, N. (2011). High-throughput, accurate mass metabolome profiling of cellular extracts by flow injection-time-of-flight mass spectrometry. Anal. Chem. *83*, 7074–7080.

Gazzerro, P., Proto, M.C., Gangemi, G., Malfitano, A.M., Ciaglia, E., Pisanti, S., Santoro, A., Laezza, C., and Bifulco, M. (2012). Pharmacological actions of statins: a critical appraisal in the management of cancer. Pharmacol. Rev. *64*, 102–146.

Hankir, M.K., Kranz, M., Keipert, S., Weiner, J., Andreasen, S.G., Kern, M., Patt, M., Kloting, N., Heiker, J.T., Brust, P., et al. (2017). Dissociation between brown adipose tissue (18)F-FDG uptake and thermogenesis in uncoupling protein 1-deficient mice. J. Nucl. Med. *58*, 1100–1103.

Hanssen, M.J., Hoeks, J., Brans, B., van der Lans, A.A., Schaart, G., van den Driessche, J.J., Jorgensen, J.A., Boekschoten, M.V., Hesselink, M.K., Havekes, B., et al. (2015). Short-term cold acclimation improves insulin sensitivity in patients with type 2 diabetes mellitus. Nat. Med. *21*, 863–865.

Iwen, K.A., Backhaus, J., Cassens, M., Waltl, M., Hedesan, O.C., Merkel, M., Heeren, J., Sina, C., Rademacher, L., Windjager, A., et al. (2017). Cold-induced brown adipose tissue activity alters plasma fatty acids and improves glucose metabolism in men. J. Clin. Endocrinol. Metab. *102*, 4226–4234.

Janmahasatian, S., Duffull, S.B., Ash, S., Ward, L.C., Byrne, N.M., and Green, B. (2005). Quantification of lean bodyweight. Clin. Pharmacokinet. *44*, 1051–1065.

Jespersen, N.Z., Larsen, T.J., Peijs, L., Daugaard, S., Homoe, P., Loft, A., de Jong, J., Mathur, N., Cannon, B., Nedergaard, J., et al. (2013). A classical brown adipose tissue mRNA signature partly overlaps with brite in the supraclavicular region of adult humans. Cell Metab. *17*, 798–805.

Jiang, Z., Yu, B., and Li, Y. (2016). Effect of three statins on glucose uptake of cardiomyocytes and its mechanism. Med. Sci. Monit. *22*, 2825–2830.

Kalinovich, A.V., de Jong, J.M., Cannon, B., and Nedergaard, J. (2017). UCP1 in adipose tissues: two steps to full browning. Biochimie *134*, 127–137.

Kazak, L., Chouchani, E.T., Jedrychowski, M.P., Erickson, B.K., Shinoda, K., Cohen, P., Vetrivelan, R., Lu, G.Z., Laznik-Bogoslavski, D., Hasenfuss, S.C., et al. (2015). A creatine-driven substrate cycle enhances energy expenditure and thermogenesis in beige fat. Cell *163*, 643–655.

Klein, J., Fasshauer, M., Klein, H.H., Benito, M., and Kahn, C.R. (2002). Novel adipocyte lines from brown fat: a model system for the study of differentiation, energy metabolism, and insulin action. Bioessays *24*, 382–388.

Klepac, K., Kilic, A., Gnad, T., Brown, L.M., Herrmann, B., Wilderman, A., Balkow, A., Glode, A., Simon, K., Lidell, M.E., et al. (2016). The Gq signalling pathway inhibits brown and beige adipose tissue. Nat. Commun. *7*, 10895.

Lasar, D., Rosenwald, M., Kiehlmann, E., Balaz, M., Tall, B., Opitz, L., Lidell, M.E., Zamboni, N., Krznar, P., Sun, W., et al. (2018). Peroxisome proliferator activated receptor gamma controls mature brown adipocyte inducibility through glycerol kinase. Cell Rep. *22*, 760–773.

Li, W., Liang, X., Zeng, Z., Yu, K., Zhan, S., Su, Q., Yan, Y., Mansai, H., Qiao, W., Yang, Q., et al. (2016). Simvastatin inhibits glucose uptake activity and GLUT4 translocation through suppression of the IR/IRS-1/Akt signaling in C2C12 myotubes. Biomed. Pharmacother. *83*, 194–200.

Li, X., Cui, Q., Kao, C., Wang, G.J., and Balian, G. (2003). Lovastatin inhibits adipogenic and stimulates osteogenic differentiation by suppressing PPARgamma2 and increasing Cbfa1/Runx2 expression in bone marrow mesenchymal cell cultures. Bone *33*, 652–659.

Lidell, M.E., Betz, M.J., Dahlqvist Leinhard, O., Heglind, M., Elander, L., Slawik, M., Mussack, T., Nilsson, D., Romu, T., Nuutila, P., et al. (2013). Evidence for two types of brown adipose tissue in humans. Nat. Med. *19*, 631–634.

Mauser, W., Perwitz, N., Meier, B., Fasshauer, M., and Klein, J. (2007). Direct adipotropic actions of atorvastatin: differentiation state-dependent induction of apoptosis, modulation of endocrine function, and inhibition of glucose uptake. Eur. J. Pharmacol. *564*, 37–46.

McDonald, M.E., Li, C., Bian, H., Smith, B.D., Layne, M.D., and Farmer, S.R. (2015). Myocardin-related transcription factor A regulates conversion of progenitors to beige adipocytes. Cell *160*, 105–118.

Nair, A.B., and Jacob, S. (2016). A simple practice guide for dose conversion between animals and human. J. Basic Clin. Pharm. *7*, 27–31.

Nakata, M., Nagasaka, S., Kusaka, I., Matsuoka, H., Ishibashi, S., and Yada, T. (2006). Effects of statins on the adipocyte maturation and expression of glucose

transporter 4 (SLC2A4): implications in glycaemic control. Diabetologia *49*, 1881–1892.

Nedergaard, J., Bengtsson, T., and Cannon, B. (2007). Unexpected evidence for active brown adipose tissue in adult humans. Am. J. Physiol. Endocrinol. Metab. *293*, E444–E452.

Olsen, J.M., Csikasz, R.I., Dehvari, N., Lu, L., Sandstrom, A., Oberg, A.I., Nedergaard, J., Stone-Elander, S., and Bengtsson, T. (2017). beta3-Adrenergically induced glucose uptake in brown adipose tissue is independent of UCP1 presence or activity: mediation through the mTOR pathway. Mol. Metab. *6*, 611–619.

Olsson, A.G., McTaggart, F., and Raza, A. (2002). Rosuvastatin: a highly effective new HMG-CoA reductase inhibitor. Cardiovasc. Drug Rev. *20*, 303–328.

Orava, J., Nuutila, P., Lidell, M.E., Oikonen, V., Noponen, T., Viljanen, T., Scheinin, M., Taittonen, M., Niemi, T., Enerback, S., et al. (2011). Different metabolic responses of human brown adipose tissue to activation by cold and insulin. Cell Metab. *14*, 272–279.

Orava, J., Nuutila, P., Noponen, T., Parkkola, R., Viljanen, T., Enerback, S., Rissanen, A., Pietilainen, K.H., and Virtanen, K.A. (2013). Blunted metabolic responses to cold and insulin stimulation in brown adipose tissue of obese humans. Obesity (Silver Spring) *21*, 2279–2287.

Ortiz, J.A., Gil-Gomez, G., Casaroli-Marano, R.P., Vilaro, S., Hegardt, F.G., and Haro, D. (1994). Transfection of the ketogenic mitochondrial 3-hydroxy-3-methylglutaryl-coenzyme A synthase cDNA into Mev-1 cells corrects their auxotrophy for mevalonate. J. Biol. Chem. *269*, 28523–28526.

Ouellet, V., Labbe, S.M., Blondin, D.P., Phoenix, S., Guerin, B., Haman, F., Turcotte, E.E., Richard, D., and Carpentier, A.C. (2012). Brown adipose tissue oxidative metabolism contributes to energy expenditure during acute cold exposure in humans. J. Clin. Invest. *122*, 545–552.

Panayiotou, G., Paschalis, V., Nikolaidis, M.G., Theodorou, A.A., Deli, C.K., Fotopoulou, N., Fatouros, I.G., Koutedakis, Y., Sampanis, M., and Jamurtas, A.Z. (2013). No adverse effects of statins on muscle function and health-related parameters in the elderly: an exercise study. Scand. J. Med. Sci. Sports *23*, 556–567.

Perdikari, A., Leparc, G.G., Balaz, M., Pires, N.D., Lidell, M.E., Sun, W., Fernandez-Albert, F., Muller, S., Akchiche, N., Dong, H., et al. (2018). BATLAS: deconvoluting brown adipose tissue. Cell Rep. *25*, 784–797.e4.

Qiang, L., Wang, L., Kon, N., Zhao, W., Lee, S., Zhang, Y., Rosenbaum, M., Zhao, Y., Gu, W., Farmer, S.R., et al. (2012). Brown remodeling of white adipose tissue by SirT1-dependent deacetylation of Ppargamma. Cell *150*, 620–632.

Rosenwald, M., Perdikari, A., Rulicke, T., and Wolfrum, C. (2013). Bi-directional interconversion of brite and white adipocytes. Nat. Cell Biol. *15*, 659–667.

Senn, J.R., Maushart, C.I., Gashi, G., Michel, R., Lalive d'Epinay, M., Vogt, R., Becker, A.S., Muller, J., Balaz, M., Wolfrum, C., et al. (2018). Outdoor temperature influences cold induced thermogenesis in humans. Front. Physiol. *9*, 1184.

Shi, F., and Collins, S. (2017). Second messenger signaling mechanisms of the brown adipocyte thermogenic program: an integrative perspective. Horm. Mol. Biol. Clin. Investig. *31*, https://doi.org/10.1515/hmbci-2017-0062.

Shinoda, K., Ohyama, K., Hasegawa, Y., Chang, H.Y., Ogura, M., Sato, A., Hong, H., Hosono, T., Sharp, L.Z., Scheel, D.W., et al. (2015). Phosphoproteomics identifies CK2 as a negative regulator of beige adipocyte thermogenesis and energy expenditure. Cell Metab. *22*, 997–1008.

Shore, A.M., Karamitri, A., Kemp, P., Speakman, J.R., Graham, N.S., and Lomax, M.A. (2013). Cold-induced changes in gene expression in brown adipose tissue, white adipose tissue and liver. PLoS One *8*, e68933.

Sjogren, A.K., Andersson, K.M., Liu, M., Cutts, B.A., Karlsson, C., Wahlstrom, A.M., Dalin, M., Weinbaum, C., Casey, P.J., Tarkowski, A., et al. (2007). GGTase-I deficiency reduces tumor formation and improves survival in mice with K-RAS-induced lung cancer. J. Clin. Invest. *117*, 1294–1304.

Svensson, P.A., Jernas, M., Sjoholm, K., Hoffmann, J.M., Nilsson, B.E., Hansson, M., and Carlsson, L.M. (2011). Gene expression in human brown adipose tissue. Int. J. Mol. Med. *27*, 227–232.

Thai, L., Rush, J.S., Maul, J.E., Devarenne, T., Rodgers, D.L., Chappell, J., and Waechter, C.J. (1999). Farnesol is utilized for isoprenoid biosynthesis in plant cells via farnesyl pyrophosphate formed by successive monophosphorylation reactions. Proc. Natl. Acad. Sci. U S A *96*, 13080–13085.

Tharp, K.M., Kang, M.S., Timblin, G.A., Dempersmier, J., Dempsey, G.E., Zushin, P.H., Benavides, J., Choi, C., Li, C.X., Jha, A.K., et al. (2018). Actomyosin-mediated tension orchestrates uncoupled respiration in adipose tissues. Cell Metab. *27*, 602–615.e4.

van Marken Lichtenbelt, W.D., Vanhommerig, J.W., Smulders, N.M., Drossaerts, J.M., Kemerink, G.J., Bouvy, N.D., Schrauwen, P., and Teule, G.J. (2009). Cold-activated brown adipose tissue in healthy men. N. Engl. J. Med. *360*, 1500–1508.

Vigano, T., Hernandez, A., Corsini, A., Granata, A., Belloni, P., Fumagalli, R., Paoletti, R., and Folco, G. (1995). Mevalonate pathway and isoprenoids regulate human bronchial myocyte proliferation. Eur. J. Pharmacol. *291*, 201–203.

Vogt, A., Qian, Y., McGuire, T.F., Hamilton, A.D., and Sebti, S.M. (1996). Protein geranylgeranylation, not farnesylation, is required for the G1 to S phase transition in mouse fibroblasts. Oncogene *13*, 1991–1999.

Wang, Q.A., and Scherer, P.E. (2014). The AdipoChaser mouse: a model tracking adipogenesis in vivo. Adipocyte *3*, 146–150.

STAR★METHODS

KEY RESOURCES TABLE

REAGENT or RESOURCE	SOURCE	IDENTIFIER
Antibodies		
UCP1	Thermo Fisher	Cat# PA1-24894; RRID: AB_2241459
HSP90	Cell Signaling	Cat# 4877; RRID: AB_2233307
γ-TUBULIN	Sigma-Aldrich	Cat# T-5326; RRID: AB_532292
HSL	Cell Signaling	Cat# 4107; RRID: AB_2296900
phospho-HSL (Ser660)	Cell Signaling	Cat# 4126; RRID: AB_490997
AKT	Cell Signaling	Cat# 9272; RRID: AB_329827
phospho-AKT (Thr308)	Cell Signaling	Cat# 13038; RRID: AB_2629447
CREB	Cell Signaling	Cat# 9197; RRID: AB_331277
phospho-CREB (Ser133)	Cell Signaling	Cat# 9198; RRID: AB_2561044
PGGT1B	Abcam	Cat# ab122122; RRID: AB_11129941
RABGGTB	Abcam	Cat# ab187717; RRID:AB_2751007
GAPDH	Cell Signaling	Cat# 5174; RRID: AB_10622025
cleaved Caspase 3 (Asp175)	Cell Signaling	Cat# 9661; RRID: AB_2341188
RHOA	Cell Signaling	Cat# 2117; RRID: AB_10693922
RAC1/2/3	Cell Signaling	Cat# 2465; RRID: AB_10695732
CDC42	Cell Signaling	Cat# 2466; RRID: AB_2078082
RAP1A/RAP1B	Cell Signaling	Cat# 4938; RRID: AB_2177112
Na^+/K^+ ATPase	Abcam	Cat# ab76020; RRID: AB_1310695
HMGCS2	Abcam	Cat# ab137043; RRID: AB_2749817
YAP1/TAZ	Cell Signaling	Cat# 8418; RRID: AB_10950494
PPARγ	Cell Signaling	Cat# 2443; RRID: AB_10694772
HMGCR	Abcam	Cat# ab174830; RRID: AB_2749818
anti-mouse HRP secondary	Millipore	Cat# 401253; RRID: AB_437779
anti-rabbit HRP secondary	Millipore	Cat# 401393; RRID: AB_10683386
Streptavidin-HRP	Cell Signaling	Cat# 3999; RRID: AB_10830897
Chemicals, Peptides, and Recombinant Proteins		
Hoechst 33342	Cell Signaling	Cat# 4082
Bodipy 493/503	Invitrogen	Cat# D3922
Syto60	Invitrogen	Cat# S11342
3-Isobutyl-1-methylxanthine	Sigma-Aldrich	Cat# I5879
Dexamethasone	Sigma-Aldrich	Cat# D4902
Indomethacin	Sigma-Aldrich	Cat# I7378
Insulin	Sigma-Aldrich	Cat# I9278
Rosiglitazone	Adipogen	Cat# 71740
Triiodo-L-Thyronine (T3)	Sigma-Aldrich	Cat# T6397
CL-316,243	Sigma-Aldrich	Cat# C5976
Collagen, Type I	Sigma-Aldrich	Cat# C3867
DMEM, low glucose	Lonza	Cat# BE12-707F
Ham's F12 medium	Lonza	Cat# BE12-615F
Penicillin-Streptomycin	Gibco	Cat# 15070063
DMEM, high glucose	Gibco	Cat# 41965062
L-glutamine	Gibco	Cat# 25030-024
Trizol reagent	Invitrogen	Cat# 15596026
DNase I (RNase-free)	NEB	Cat# M0303
Simvastatin	Sigma-Aldrich	Cat# S6196

(*Continued on next page*)

Continued

REAGENT or RESOURCE	SOURCE	IDENTIFIER
Fluvastatin	Sigma-Aldrich	Cat# SML0038
Atorvastatin	Sigma-Aldrich	Cat# PZ0001
Rosuvastatin	Sigma-Aldrich	Cat# SML1264
Pravastatin	Sigma-Aldrich	Cat# P4498
Cerivastatin	Sigma-Aldrich	Cat# SML0005
GGTI-298	Sigma-Aldrich	Cat# G5169
FTI-277	Sigma-Aldrich	Cat# F9803
Farnesyl pyrophosphate	Sigma-Aldrich	Cat# F6892
Farnesol	Abcam	Cat# ab142428
Geranylgeranyl pyrophosphate	Sigma-Aldrich	Cat# G6025
Geranylgeraniol	Abcam	Cat# ab142436
Gallein	Santa Cruz	Cat# sc-202631
Rho inhibitor, Rhosin	Calbiochem	Cat# 555460
Squalene	Sigma-Aldrich	Cat# S3626
Coenzyme Q9	Sigma-Aldrich	Cat# 27597
Coenzyme Q10	Sigma-Aldrich	Cat# C9538
Tamoxifen	Sigma-Aldrich	Cat# T5648
4-Hydroxytamoxifen	Sigma-Aldrich	Cat# H7904
D-glucose	Sigma-Aldrich	Cat# G7021
Oligomycin	Adipogen	Cat# 11342
Isoproterenol	Sigma-Aldrich	Cat# I5627
Dibutyryl-cAMP	Sigma-Aldrich	Cat# D0627
FCCP	Sigma-Aldrich	Cat# C2920
Rotenone	Sigma-Aldrich	Cat# R8875
Antimycin A	Sigma-Aldrich	Cat# A8674
Sodium pyruvate	Invitrogen	Cat# 11360070
Seahorse XF Base Medium	Agilent	Cat# 102353
Complete Protease Inhibitors	Roche	Cat# 05056489001
Halt Phosphatase Inhibitors	ThermoFischer	Cat# 78426
Click-IT Geranylgeranyl Alcohol, Azide	Invitrogen	Cat# C10249
Biotin Alkyne	Invitrogen	Cat# B10185
Phalloidin-iFluor 488 Reagent	Abcam	Cat# ab176753
Critical Commercial Assays		
High Capacity cDNA RT kit	Applied Biosystems	Cat# 4368814
TruSeq RNA library prep kit	Illumina	Cat# RS-122-2301
DC Protein Assay	Bio-Rad	Cat# 5000111
Click-IT Protein Reaction Kit	Invitrogen	Cat# C10276
XFE96 FluxPak	Agilent	Cat# 102416-100
Glycerol reagent	Sigma-Aldrich	Cat# F6428
QBT fatty acid uptake assay kit	Molecular Devices	Cat# R6132
Luciferase reporter system	Promega	Cat# E1501
Autokit Total Ketone Bodies R1 Set	Wako Chemicals	Cat# 415-73301
Autokit Total Ketone Bodies R2 Set	Wako Chemicals	Cat# 413-73601
Deposited Data		
RNA sequencing data for clinical transcriptome study	European Nucleotide Archive	PRJEB23275
Experimental Models: Cell Lines		
immortalized brown adipocytes	Christian Wolfrum	Klein et al., 2002
hMADS cells	Ez-Zoubir Amri	Elabd et al., 2009

(*Continued on next page*)

Continued

REAGENT or RESOURCE	SOURCE	IDENTIFIER
Experimental Models: Organisms/Strains		
C57BL/6N mice	Charles River	C57BL/6NCrl Strain code 027
Ucp1-CreERT2 x LoxP-Red mice	Christian Wolfrum	Rosenwald et al., 2013
Pggt1b$^{fl/fl}$ mice	Martin Bergo	Sjogren et al., 2007
Adip-CreERT2 mice	Christian Wolfrum	Rosenwald et al., 2013
Oligonucleotides		
qPCR primers	Microsynth	Listed in Table S4
siRNAs	Microsynth	Listed in Table S3
Software and Algorithms		
Harmony - Operetta software	Perkin Elmer	version 3.5
ImageJ	NIH, USA	version 1.50b
Phenomaster software	TSE systems	version 5.6.5
Wave - XF96 software	Agilent	version 2.3.0.19
ImageQuant LAS 4000	GE Healthcare	version 1.1
GraphPad Prism 7	GraphPad software	version 7.03
ViiA7 software	Applied Biosystems	version 1.2.3
Gen5	BioTek	version 1.10

CONTACT FOR REAGENT AND RESOURCE SHARING

Further information and requests for resources and reagents should be directed to and will be fulfilled by the Lead Contact, Professor Christian Wolfrum (christian-wolfrum@ethz.ch).

EXPERIMENTAL MODEL AND SUBJECT DETAILS

Clinical Transcriptome Study

The clinical study was approved by the Local Ethics Committee of the University Hospital in Bratislava, Slovakia and it conforms to the ethical guidelines of the 2000 Helsinki declaration. All study participants provided witnessed written informed consent prior entering the study. Deep neck brown and adjacent subcutaneous white adipose tissue samples were obtained from the lower third of the neck by an experienced ENT surgeon during neck surgery under general anesthesia. The deep neck adipose tissue sample was taken from pre- and paravertebral space between common carotid and trachea in case of thyroid surgery and just laterally to carotid sheath in case of branchial cleft cyst surgery. In all cases, the surgical approach was sufficient to reach and sample the deep neck adipose tissue without any additional morbidity. Patients with malignant disease and subjects younger than 18 years were excluded from participation in the study. Adipose tissue samples were immediately cleaned from blood and connective tissue, and frozen in liquid nitrogen until further processing. In order to identify patients with active BAT, we first quantified expression of brown adipocyte marker genes in individual biopsies using qPCR. By analyzing BAT and WAT biopsies of 18 patients, we identified 10 individuals with active BAT (2 male/8 female; 39.6 ± 4.7 years; BMI 23.5 ± 0.8 kg/m^2; waist circumference 82.5 ± 4.3 cm; body fat 28.2 ± 2.0 %; thyroid surgery n=9 or branchial cleft cyst surgery n=1). Adipose tissue biopsies of these patients were subjected to RNA sequencing. Our cohort consists of 2 male and 8 female patients, which is mainly due to the fact that prevalence of BAT is higher in females than in males and also because more females were willing to participate in our study. We have analyzed BAT and WAT transcriptomes of all patients and could not find any difference between male and female tissues in Principal component analysis (Perdikari et al., 2018).

Retrospective ^{18}FDG-PET/CT Cohort Study

The retrospective study was approved by the ethics committee of the canton of Zurich. 8409 ^{18}FDG-PET scans were reviewed of patients who had been hospitalized in the winter months (Nov-Feb) at University Hospital of Zürich between November 2009 and February 2015. Of those, 2789 patients (1105 female/1684 male; mean age 60.0 ± 14.8 years; mean BMI 24.5 ± 4.9 kg/m^2) were identified who had been hospitalized up to 12 months prior to the scan (median time to PET: 4.7 months) and had electronic patient files available. All scans were manually reviewed by specialized physicians for presence of active BAT, which was graded using a previously published anatomical system (Becker et al., 2016). Electronic patient files were searched for administered medication of the class of statins. Statistical analysis was performed with R version 3.4.4. The formula for the general linear model was 'BAT-Grade'[0-3] ~ Statin[binary] * age * BMI * sex. Step-wise model selection was performed with the function *stepAIC* from the package

MASS version 7.3-50. The according scatterplot was created with the package *ggplot2* version 2.2.1. Both males and females were included in the analysis, however, statin use was significantly associated with BAT inactivity even after adjustment for sex, age and BMI (Table S1).

Clinical Fluvastatin Study

The clinical study was approved by the ethics committee of the canton of Zurich. The study is registered under the ClinicalTrials.gov identifier NCT03189511, where the detailed study protocol can be accessed. In short, 16 healthy male Caucasian volunteers with a BMI of 19-27 kg/m^2 (23.1±1.7 kg/m^2) and between 18 to 50 years of age (25.1±1.4 years) were included. We have focused on males in a non-overweight BMI range to reduce the variability of the observed effects. In female volunteers a potential variability for the menstrual cycle would have to be accounted for. In addition, the inclusion of female volunteers would include the need for negative pregnancy tests and safe contraception during the study period, since this study involved ionizing radiation. For a power of 80%, at a type one error level of 5% a minimal sample size of 10 participants is needed to detect a significant difference (50% drop in activity). In order to account for heterogeneity of the sample and dropouts, we recruited 16 participants. All participants were first screened by indirect calorimetry for an increase in cold-induced thermogenesis of at least 5% of resting energy expenditure at warm conditions. The schedule of both study visits spaced 14 days apart was identical: The volunteer arrived in a fasted state for oral administration of 200mg Mirabegron (Betmiga, Astellas Pharma, Switzerland). Volunteers were given standard hospital gowns for the entire duration of the study visit. After 90 minutes waiting time, standardized cold stimulation with water cooling pads (Hilotherm Clinic; 10°C setting) was commenced lasting another 120 minutes. Skin and room temperatures were monitored with surface temperature probes. No shivering was reported by any of the participants. At the end of the cooling period the participant was transferred to the PET/MR table (SIGNA PET/MR, GE Healthcare, Waukesha, WI, USA). The scan procedure was performed by experienced technicians and were compliant with EANM standards. Low blood sugar (<7 mM) was confirmed with a finger prick blood test. For the scan, the participants received 75 MBq of ^{18}FDG intravenously via the antecubital vein, with immediately following partial-body (vertex to mid-torso) PET/MR scan for 50±10 minutes. All scans were performed in the afternoon (between 2-4 pm). SUVlean was calculated using the Janmahasatian formulation (Janmahasatian et al., 2005). After the scan, the location of metabolically active brown fat in the supraclavicular region was determined qualitatively on the PET/MR images and targeted by an ultrasound-guided coaxial core-needle (16G size, 10mm core length, BARD Mission) biopsy under local anesthesia. Samples (~1-2 mg) were immediately frozen in dry ice. Volunteers remained in a fasted state until after the biopsy. At the end of the 1st visit, volunteers received the study medication and instructions for the intake over the next 14 days, until the 2nd study visit (2x40mg fluvastatin daily per os). The core-needle biopsy on the second visit was performed through the same access point as the first one, with the same anatomical landmarks with the help of a screenshot of the first biopsy (representative example in Figures S7A–S7D), and with the same depth of needle insertion (if possible), in order to ensure sampling as close as possible to the location of the first biopsy. Two volunteers were excluded from the analysis, one due to non-compliance (no change in cholesterol levels) and in the second we failed to obtain sufficient amount of tissue for the gene expression analysis.

Mouse Experiments

All animal procedures were approved by the Veterinary office of the Canton of Zürich. Sample size was determined based on previous experiments in our lab and similar studies reported in the literature. All mice used for the experiments were male, housed 3-4 littermates per cage in individually ventilated cages at standard housing conditions (22°C, 12 h reversed light/dark cycle, dark phase starting at 7am), with *ad libitum* access to chow (18 % proteins, 4.5 % fibers, 4.5 % fat, 6.3 % ashes, Provimi Kliba SA) and water. Health status of all mouse lines were regularly monitored according to FELASA guidelines. 12-14 weeks old male C57Bl6 mice (Charles River) were subjected to statins (10 mg/kg/day) or GGTI-298 (1 mg/kg/day) treatment for 6 consecutive days by oral gavage or intraperitoneal injection, respectively. Mice were kept for 2 days at 22°C, followed by 4 days of cold exposure at 8°C, or 2 days of CL-316.243 injection (0.1 mg/kg/day) to activate thermogenesis. GGOH (50 mg/kg/day) was administered to 10-week old C57Bl6 mice housed at 22°C for 4 consecutive days by IP injection. Neither acute cold exposure nor CL-316.243 was applied to investigate the effect of GGOH on browning of iWAT.

Pggt1b$^{fl/fl}$ mice (Sjogren et al., 2007) were crossed to *Adip*-CreERT2 mice (Rosenwald et al., 2013) to achieve inducible adipocyte-specific ablation of GGTase I. At 12 weeks of age, recombination of the floxed allele was induced by oral tamoxifen gavage (2mg/day in sunflower oil, Sigma-Aldrich). To induce thermogenesis, mice were injected with CL-316.243 (IP 0.1 mg/kg/day) or exposed to 8°C. All studies were performed on 12-14 week old male mice. In high fat diet cohorts (23.9 % proteins, 4.9 % fibers, 35 % fat, 5.0 % ashes, Provimi Kliba SA), the feeding regimen (8 weeks) was initiated at age of 6 weeks.

The *Ucp1*-tracer mouse line (*Ucp1*-CreERT2 x LoxP-Red) was previously described (Rosenwald et al., 2013). To investigate the effect of statins on the number of UCP1$^+$ cells, 14-week old male mice were treated with fluvastatin (10 mg/kg/day) by IP injection for 6 consecutive days. First two days, mice were kept at 22°C to achieve inhibition of mevalonate pathway before they were moved to 8°C (days 3-6). To induce CreERT2 activity, mice were injected with tamoxifen (day 3-4, 2 mg/day).

Cell Culture – hMADS Cells

HMADS cells originating from the prepubic fat pad of a 4-month-old male were kindly provided by Dr. Amri and cultured as previously described (Elabd et al., 2009). Briefly, cells (between passage 14 and 16) were grown in low glucose DMEM supplemented with 15mM HEPES, 10% FBS, 2mM L-glutamine, 1% Penicillin/Streptomycin and 2.5ng/ml recombinant human FGF-2 (Peprotech) in

normoxic humidified cell culture incubator (5% CO_2 and 37°C). The medium was changed every other day and FGF-2 was omitted after cells reached confluence. Differentiation of 48 hours post-confluent cells was induced (day 0) by adipogenic medium (DMEM/Ham's F12 media (Lonza) containing 10μg/ml Transferrin, 10nM insulin and 0.2nM triiodothyronine) supplemented with 1μM dexamethasone and 500μM isobutyl methylxanthine (IBMX) and from day 2 to 9, cells were cultured in adipogenic medium containing 100nM rosiglitazone. All compounds were obtained from Sigma-Aldrich (specification in Key Resources Table), except for rosiglitazone (Adipogen). Cells were kept in culture until day 18 in absence of rosiglitazone to obtain mature white adipocytes. To obtain brown adipocytes, cells were exposed to an additional rosiglitazone pulse between days 14 - 18. To investigate the effect of pharmacological agents on browning of white adipocytes, treatment was performed between day 14 and 18 in combination with rosiglitazone. To knockdown candidate genes, 50nM siRNA pools (Microsynth) were delivered into mature adipocytes on day 13 using Lipofectamine RNAiMAX (Invitrogen) according to manufacturer's instructions. A control siRNA pool was used in all experiments as a control. To make sure that the observed phenotypes are not due to off-target effects of the control siRNA pool, we validated the critical experiments using scrambled siRNA pools (Figures S7E–S7J). All siRNA sequences and corresponding knockdown efficiencies are listed in Table S3. After 24 hours, transfection medium was replaced by fresh adipogenic medium containing 100nM rosiglitazone. Adipocytes were cultured until day 18, when cellular respiration was determined or cells were harvested for RNA and protein analysis. All cell lines used were regularly tested negative for mycoplasma contamination throughout the whole duration of this study.

Cell Culture – Immortalized Murine Brown Adipocytes

Preadipocytes isolated from the iBAT stromal-vascular fraction of late fetal and newborn C57Bl/6 mice (both genders) and immortalized by introducing the SV40 antigen were kindly provided by Prof. Klein (Klein et al., 2002). Preadipocytes (between passage 4 and 6) were grown on collagen-coated plates in DMEM containing 10% FBS and 1% Pen/Strep (Gibco) in normoxic humidified cell culture incubator (5% CO_2 and 37°C). After reaching confluence, adipogenic differentiation was induced by supplementing the medium with IBMX (500μM), dexamethasone (1μM), insulin (20nM), T3 (1nM) and indomethacin (125μM). All compounds were obtained from Sigma-Aldrich (specification in Key Resources Table). After 48 hours, medium was replaced by fresh maintenance medium containing (insulin and T3), which was replaced every other day. For siRNA-mediated knockdown, differentiating adipocytes (day 5) were trypsinized, counted and replated on collagen-coated multi-well plates to reduce cell density. Cells were allowed to attach, recover and maturate before siRNA transfection (100nM siRNA pools, day 6) or treatment with different compounds (day 7). Cells were harvested on day 9 for RNA and protein analysis, or cellular respiration measurements. All siRNA sequences are listed in Table S3. All cell lines used were regularly tested negative for mycoplasma contamination throughout the whole duration of this study.

METHOD DETAILS

Intraperitoneal Glucose Tolerance Test

To measure glucose tolerance, mice were fasted for 6 hours by removal to a clean cage without food at the end of the dark (active) phase. Mice were weighed and after fasting glucose levels were obtained from a small tail clip using a standard glucometer (ACCU-CHEK Aviva, Roche), D-glucose (Sigma-Aldrich) was injected intraperitoneally at dose 1 mg/g body weight. Blood glucose levels were measured 15, 30, 60 and 120 minutes after glucose injection using glucometer.

Body Composition Measurement

Live mice body composition was measured with a magnetic resonance imaging technique (EchoMRI 130, Echo Medical Systems). Mice were fasted for 4 hours before measurement. Fat and lean mass was analyzed using Echo MRI 14 software.

Indirect Calorimetry

Indirect calorimetry measurements were performed with the Phenomaster (TSE Systems) according to the manufacturer's guidelines. O_2 and CO_2 levels were measured for 60s every 13 minutes continuously. Energy expenditure was calculated according to the manufacturer's guidelines. The respiratory quotient was estimated by calculating the ratio of CO_2 production to O_2 consumption. Animals were single-caged and acclimated to the metabolic cage for 48 hours prior metabolic recording. Locomotor activity, food and water intake were monitored throughout the whole measurement.

Tissue Harvest

Animals were euthanized singly in carbon dioxide atmosphere. All tissues were carefully dissected, weighed and snap frozen in liquid nitrogen until further processing. Popliteal lymph nodes were carefully removed from iWAT for all gene and protein expression analyses. For RNA and protein isolation, whole adipose tissue depot was homogenized.

Analysis of Preadipocyte Proliferation and Adipocyte Differentiation

To study the effect of statins on preadipocyte proliferation, immortalized murine preadipocytes were plated on 96-well Operetta plates at low density (2.000 cells/cm^2) and allowed to attach and recover for 12 hours. Cells were treated for 48h with atorvastatin, cerivastatin, simvastatin, fluvastatin and rosuvastatin (all statins were purchased from Sigma-Aldrich) at two different concentrations (1 and 10μM). Cells were fixed with 4% formaldehyde for 20 min and washed 3 times with PBS. Immediately after washing, cells were

stained with Hoechst (Cell Signaling) and Syto60 (Invitrogen), to visualize nuclei and cytosol, respectively. Differentiated adipocytes at day 9 were used for differentiation analysis. Briefly, cells in 96-well optical plate, exposed to statins for the last 48 hours (day 7-9), were fixed with 4% formaldehyde for 20 min and washed 3 times with PBS. Immediately after washing, cells were stained with Bodipy (Invitrogen) for lipid droplets and Hoechst (Cell Signaling) for nuclei. Twenty-five pictures per well were taken with an automated microscope imaging system (Operetta, PerkinElmer). Pictures were analyzed using the Harmony software. In differentiation assay, all cells (Hoechst stained nuclei) surrounded by lipid droplets were considered adipocytes. In proliferation assay, nuclei were counted.

Cellular Respiration

For measurement of cellular respiration, immortalized murine brown adipocytes were cultured on collagen-coated cell culture dishes. Differentiating adipocytes were trypsinized and replated on day 5 at density 7.000 cells per well and allowed to recover for 48 hours before treatment. Since hMADS cells grow in a monolayer, they were differentiated directly on collagen-coated 96-well Seahorse microplates. On the day of experiment, adipogenic medium was replaced with XF Assay Medium (pH 7.4, Seahorse Bioscience) supplemented with glucose (1g/L; Sigma-Aldrich), 2mM sodium pyruvate (Invitrogen) and 2mM L-glutamine (Invitrogen). The oxygen consumption rate (OCR) was measured using the Extracellular flux analyzer XF96 (Agilent). Test compounds were sequentially injected to obtain following concentrations: 1μg/ml Oligomycin, 1μM isoproterenol, (0.5mM dibutyryl cAMP for hMADS), 1μg/ml FCCP, 3μM Rotenone with 2μg/ml Antimycin A. All compounds were purchased from Sigma-Aldrich, except for Oligomycin (Adipogen). OCR levels (pmol/min) were normalized to protein amount per well (μg protein). Non-mitochondrial respiration was subtracted to obtain basal, basal uncoupled, stimulated uncoupled and maximal mitochondrial respiration.

Fatty Acid Uptake

Fatty acid uptake was measured by a fluorescence-based assay utilizing BODIPY dodecanoic acid fluorescent fatty acid analogue (QBTTM Fatty Acid Uptake Assay kit, Molecular Devices, USA). Briefly, the cells were fasted for 2 hours in serum free culture media prior analysis. Isoproterenol (1μM; Sigma-Aldrich) was added and plate was incubated for another 30 minutes at 37°C in humidified CO_2 incubator. After stimulation, the cells were loaded with fatty acid analogue according to manufacturer's instructions and uptake kinetics was measured every 30s for 30 min with λex = 485 nm and λem = 515 nm using the microplate reader Synergy MX and Gen5 software (BioTek). Linear phase of fluorescence signal corresponding to fatty acid uptake was used for calculation after normalization to background fluorescence and protein content. The data are presented as relative fluorescence per μg protein per minute.

Lipolysis

Lipolytic activity of mature brown adipocytes was determined as glycerol release into culture media. Briefly, the cells were serum starved for 2 hours in low-glucose medium (Gibco) prior to the analysis. Isoproterenol (1μM; Sigma-Aldrich) was added and plate was incubated for another 30 minutes at 37°C in humidified CO_2 incubator. Media were collected and spun down to pellet detached cells. Glycerol was assessed in the supernatant using the Glycerol reagent (Sigma-Aldrich) according to manufacturer's instructions and normalized to protein content in the well. Absorbance (at 540 nm) was measured using the microplate reader Synergy MX and Gen5 software (BioTek).

Glucose Uptake

Glucose uptake in mature brown adipocytes was determined as the amount of ^{14}C-2-deoxyglucose taken up by cells per minute. Briefly, cells were starved in low glucose DMEM (Gibco) for 2 hours. Starved cells were washed twice warm PBS and incubated at 37°C in low glucose DMEM for additional 50 minutes. Isoproterenol (1μM) was added to assess isoproterenol stimulated glucose uptake. Cells were washed twice with fresh Krebs–Ringer-HEPES buffer (50 mM HEPES, 137 mM NaCl, 4.7 mM KCl, 1.85 mM $CaCl_2$, 1.3 mM $MgSO_4$, pH 7.4) containing 0.1% fatty acid-free BSA and incubated in presence of ^{14}C-2-deoxyglucose (0.1 μCi/well; PerkinElmer) for exactly 10 minutes. Cells were washed 4 times with ice cold PBS and lysed in 0.1M NaOH. Lysates were mixed with 3 ml scintillation cocktail and radioactivity was quantified in disintegrations per minute (DPM) using the Liquid Scintillation Analyzer TRI-CARB 2000CA (PerkinElmer) and normalized to protein content in the corresponding well.

Ketone Bodies Measurement

Levels of ketone bodies in cell lysate and cell-conditioned media were determined using a commercially available kit according to manufacturer's instructions (Wako Chemicals) and normalized to protein amount.

Ucp1 Promoter Activity

Ucp1 promoter activity was determined in a murine immortalized brown adipocytes expressing Luciferase under *Ucp1* promoter. Preadipocytes were cultured on collagen-coated plates in DMEM containing 10% FBS and 1% Pen/Strep (Gibco). Adipogenic differentiation was induced by supplementing the medium with IBMX (500μM), dexamethasone (1μM), insulin (20nM), T3 (1nM) and indomethacin (125μM) 2 days after reaching confluence. After 48 hours, medium was replaced by fresh maintenance medium containing 20nM insulin, 1nM T3 and 1μM 4-hydroxytamoxifen (to induce Cre), which was replaced every other day. All compounds were purchased from Sigma-Aldrich. The cells were treated with different concentration of simvastatin from day 7 for 48 hours. On day 9, cells were washed with PBS, lysed in passive lysis buffer and luciferase activity was measured using Dual Luciferase Reporter Assay (Promega) on Synergy MX (BioTek) and normalized to protein content.

RNA Extraction, cDNA Synthesis, Quantitative RT-PCR

Total RNA was extracted from tissues or cells using Trizol reagent (Invitrogen) according to the manufacturer's instructions. DNase treatment (NEB BioLabs) was included to remove traces of genomic DNA. Reverse transcription was performed to generate cDNA library by using the High Capacity cDNA Reverse transcription kit (Applied Biosystems), with 1μg of RNA. Quantitative PCR was performed on a ViiA7 (Applied Biosystems) and relative mRNA concentrations normalized to the expression of *RPL13A1* (human fat samples) or *TBP* (cell culture) were calculated by the ΔΔCt method. Primer sequences are found in Table S4.

Protein Extraction and Western Blot

Adipose tissue samples and *in vitro* differentiated adipocytes were homogenized in RIPA buffer (50mM Tris-HCl pH 7.4, 150mM NaCl, 2mM EDTA, 1.0% Triton X100, 0.5% sodium deoxycholate) supplemented with protease (Complete, Roche) and phosphatase (Halt phosphatase inhibitor cocktail, ThermoFisher) inhibitor cocktails. Lysates were cleared by centrifugation at 12,000g for 15 minutes at 4°C. Protein concentration of the supernatants was determined by DC Protein Assay (Bio-Rad). Equal amount of proteins (5-20 μg) were separated on 12% SDS-polyacrylamide gel, transferred to a nitrocellulose membrane (Bio-Rad) and stained for UCP1 (1:1000, Pierce), phospho-HSL (Ser660; 1:1000, Cell Signaling), total HSL, phospho-CREB (Ser133; 1:1000, Cell Signaling), total CREB (1:1000, Cell Signaling), phospho-AKT (Thr308; 1:1000, Cell Signaling), AKT (1:1000, Cell Signaling), HMGCS2 (1:1000, Abcam), HMGCR (1:1000, Abcam), cleaved Caspase 3 (1:1000, Cell Signaling), GAPDH (1:1000, Cell Signaling), Na^+/K^+ ATPase (1:10.000, Abcam), PPARγ (1:1000, Cell Signaling), RHOA (1:1000, Cell Signaling), RHO (1:1000, Cell Signaling), CDC42 (1:1000, Cell Signaling), RAP1A/B (1:1000, Cell Signaling), RAC1/2/3 (1:1000, Cell Signaling), PGGT1B (1:1000, Abcam), RABGGTB (1:1000, Abcam), YAP1/TAZ (1:1000, Cell Signaling), HSP90 (1:1000, Cell Signaling) and γ-tubulin (1:10.000, Sigma-Aldrich). Signal of the HRP-conjugated secondary antibodies (1:10.000, Calbiochem) was visualized by the Image Quant system (GE Healthcare Life Sciences). All antibodies are listed in the Key Resources Table.

Click Chemistry

To identify proteins incorporating the geranylgeranyl group, mature immortalized brown adipocytes were treated for 24 h with simvastatin to block mevalonate pathway and endogenous GGPP production. Maintenance medium was supplemented with GGOH (Abcam) or geranylgeranyl alcohol azide (Invitrogen) and cells were allowed to incorporate the regular/labeled isoprenoid group for 24 hours. Cells were washed 3 times with PBS, scraped in ice-cold RIPA buffer and extracted proteins were precipitated using methanol/chloroform. Proteins were resuspended in 0.1M Tris-HCl (pH 8.0) containing 1% SDS. The click reaction was performed using the Click labeling kit (Invitrogen) according to manufacturer's instructions. Biotin-alkyne was used as substrate for this reaction. Proteins were precipitated and washed to remove unbound biotin, dissolved in Laemmli buffer, heat denaturated for 10 minutes at 70°C and separated on PAGE. Proteins were transferred to nitrocellulose membrane and geranylgeranyl-biotin complexes were detected using Streptavidine-HRP (Cell Signaling).

Subcellular Fractionation

In order to analyze subcellular distribution of small GTP-binding proteins, cells were fractionated using differential centrifugation. Mature adipocytes cultured on P10 dishes were treated with statins or GGTI-298 inhibitor, washed 3 times with ice-cold PBS and scraped in fractionation buffer (250mM Sucrose, 20mM HEPES (pH 7.4), 10mM KCl, 1.5mM $MgCl_2$, 1mM EDTA, 1mM EGTA) supplemented with 1mM DTT (Sigma-Aldrich) protease (Complete, Roche) and phosphatase (Halt phosphatase inhibitor cocktail, Thermo Fisher) inhibitors cocktails. Cells were passed through a 25 gauge needle 10 times and incubated on ice for 20 min. In the first centrifugation step (500g/5min/4°C) nuclei were pelleted. Supernatant containing cytosol, membranes and organelles was transferred into a clean Eppendorf tube and centrifuged (10,000g/5min/4°C) to pellet mitochondria and other organelles. Supernatant containing cytosol and membranes was transferred into an ultracentrifugation tube and membranes were pelleted by ultracentrifugation (100,000g/60min/4°C; Optima MAX-XP, Beckman Coulter). Supernatant was saved as cytosolic fraction. After washing the membrane pellet twice with fresh fractionation buffer, pellet containing membranes was resuspended in ice-cold RIPA buffer.

F-actin Staining

F-actin was stained in both cell lines using Phalloidin-iFluor 488 Reagent (Abcam). Cells were treated with statins for 48 hours, washed with PBS and fixed 20 minutes with 4% Formaldehyde (Sigma-Aldrich). Fixed cells were permeabilized for 5 minutes using 0.1% Triton and washed 3 times with PBS. F-actin fibers were stained for 1 hour with Phalloidin dye diluted 1:1000 in PBS with 0.1% BSA (Sigma-Aldrich). Nuclei were stained in parallel using Hoechst (Cell Signaling). After cells were washed 3 times with PBS, pictures were obtained using the automated Operetta imaging system (PerkinElmer).

RNA Sequencing, Mapping and Analysis

RNA extracted from brown and white adipose tissue biopsies was quality checked by Tapestation (Agilent). All samples had a RIN value of greater than 8. For the preparation of libraries the TruSeq mRNA sample preparation kit (Illumina) was used. Sequencing was performed as 50 bp, single reads and 7 bases index read on an Illumina HiSeq2000 instrument. Approximately 20–30 million reads per sample were obtained. The raw reads were first cleaned by removing adapter sequences, trimming low quality ends, and filtering reads with low quality (phred quality <20). Sequence alignment of the resulting high-quality reads to the human genome (build

GRCh38) and quantification of gene level expression was carried out using RSEM (version 1.2.18). To detect differentially expressed genes, we applied a count based negative binomial model implemented in the software package edgeR (R-version 3.1.2, edgeR 3.8.5). The gene-wise dispersions were estimated by conditional maximum likelihood and an empirical Bayes procedure was used to shrink the dispersions towards a consensus value. The differential expression was assessed using an exact test adapted for over-dispersed data. The genes were filtered for significant differential expression using an adjusted P-value cutoff at 0.05 (after Benjamini–Hochberg multiple testing correction).

Quantification of Cre Recombination in Mouse Tissues

Genomic DNA was prepared by following protocol. The tissue was crushed in a Thermolyser LT (Qiagen) in 1 ml 50mM NaOH. 250 μl of 1 M Tris-HCl was added to neutralize the tissue lysate. The samples were centrifuged and the supernatant was diluted in MQ water. Quantification of the number of recombined LoxP-Red and non-recombined *ApoB* genomic loci copies was performed by qPCR. Absolute standard curves were prepared from synthesized pUC57recloxPRed-ApoB plasmid. Reactions were performed with following primers at final concentration 250 nM and Fast SYBR Green master mix (Applied Biosystems). Recombined ^{fl}stop^{fl} tdRFP: FW GCGCATGAACTCTTTGATGAC, RV TCGCGGTTGAGGACAAACTC; *ApoB*: FW GTCCAGGTTGAATCACGGGT, RV AGGATCCTGCAAGGTCAAGC.

Metabolomic Analysis

For metabolomic analysis, tissue samples were weighed and homogenized in 10 volumes of extraction solvent, acetonitrile: methanol: water (40:40:20) pre-chilled to -20°C. All samples were kept on dry ice during processing. Homogenates were briefly spun down and supernatants were subjected to metabolomic analysis by flow-injection – time of flight mass spectrometry (Fuhrer et al., 2011) on an Agilent 6550 QTOF instrument. Metabolites were identified by matching measured and theoretical m/z within a tolerance of 0.001 amu.

QUANTIFICATION AND STATISTICAL ANALYSIS

For *in vivo* studies, littermates randomly assigned to treatment groups were used for all experiments. Sample sizes were determined on the basis of previous experiments using similar methodologies. The animal numbers used for all experiments are indicated in the corresponding figure legends. In the clinical transcriptomic study, only volunteers with active BAT (enrichment of brown adipocyte marker genes in BAT compared to WAT) were included. In the clinical fluvastatin trial, 2 volunteers were excluded from the analysis, one due to non-compliance (no change in cholesterol levels) and in the second we failed to obtain sufficient amount of tissue for the gene expression analysis. All animals were included in statistical analyses, and the investigators were not blinded. All cell culture experiments were performed with 2-3 technical replicates for RNA and protein analysis, 5-6 replicates for measurement of cellular respiration and *Ucp1* promoter activity, and independently reproduced 2-4 times. No Results are reported as mean ± SEM for mouse and cell culture data and mean ± SD for the clinical trial. Two-tailed unpaired Student's T-test was applied on comparison of two groups. In case of non-normal data distribution, a non-parametric Wilcoxon test was performed. ANOVA was applied on comparisons of multiple groups. Pearson's correlation coefficient was calculated and all statistical analyses were performed using GraphPad Prism 7 and R version 3.4.4. Statistical differences are indicated as * for $P < 0.05$, ** for $P<0.01$ and *** for $P<0.001$.

DATA AND SOFTWARE AVAILABILITY

The accession number for the RNA sequencing data from the clinical transcriptome study reported in this paper is The European Nucleotide Archive: PRJEB23275.